Deglaciation history at the Alpine-Mediterranean transition (Argentera-Mercantour, SW Alps) from 10Be dating of moraines and glacially polished bedrock

Y. Rolland, Romain Darnault, Regis Braucher, D.L. Bourles, Carole Petit, Stéphane Bouissou

Rolland, Y., Darnault, R., Braucher, R., Bourlès, D., Petit, C., Bouissou, S., ASTER Team, 2019. Deglaciation history at the Alpine-Mediterranean transition (Argentera-Mercantour, SW Alps) from ^{10}Be dating of moraines and glacially polished bedrock. ***Earth Surface Processes and Landforms*****. DOI: 10.1002/esp.4740**

Insights

New CRE ^{10}Be datings show that the southern slope of SW Alps experienced:

(1) A phase of upper slope (2700-2800 m a.s.l.) deglaciation at 20.8-18.6 ka, after the LGM.

(2) A major deglaciation and onset of lake sedimentation at 15.3-14.2 ka.

(3) Deglaciation following the Younger Dryas from 12 to 8-9 ka, featured by retrogressive melting of rock glaciers and moraine erosion/stabilization.

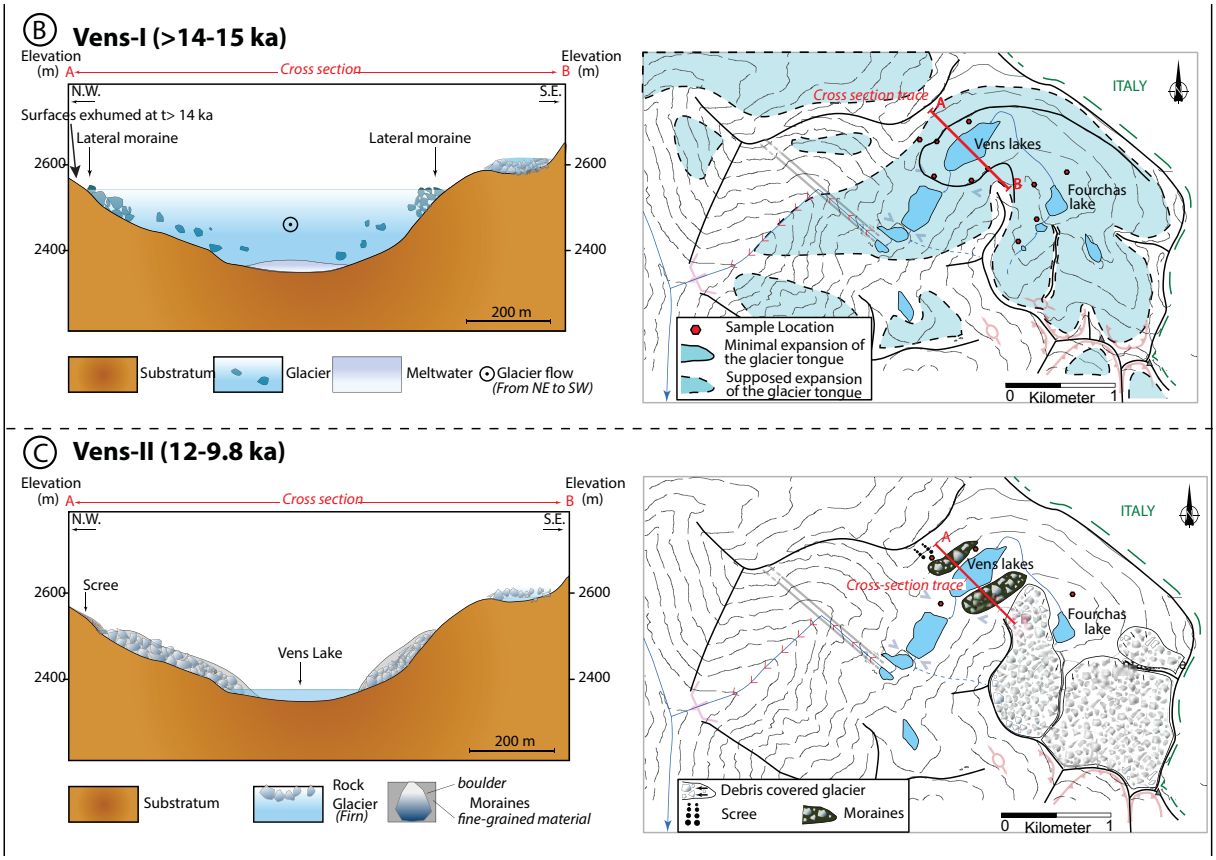

Deglaciation history at the Alpine-Mediterranean transition (Argentera-Mercantour, SW Alps) from ^{10}Be dating of moraines and glacially polished bedrock

Yann Rolland[1-2*], Romain Darnault[3], Régis Braucher[4], Didier Bourlès[4], Carole Petit[1], Stéphane Bouissou[1], ASTER Team[4,&].

[1] Univ. Savoie Mont Blanc, Univ. Grenoble Alpes, CNRS, Pôle Montagne, EDYTEM, 73376 Le Bourget-du-Lac, France.

[2] Université Côte d'Azur, CNRS, OCA, IRD, Géoazur, France.

[3] IFP Energies Nouvelles, 1 et 4 avenue de Bois-Préau, 92852 Rueil-Malmaison, France.

[4] Aix-Marseille Université, CNRS-IRD-Collège de France, CEREGE, Technopôle de l'Environnement Arbois-Méditerranée, BP80, 13545 Aix-en-Provence, France

&: Georges Aumaître and Karim Keddadouche.

*corresponding author yann.rolland@univ-smb.fr

Abstract

Estimating the extent and age of the last glacial maxima as well as the chronology of glacial recessions in various environmental contexts is key to source-to-sink studies and paleoclimate reconstructions. The Argentera-Mercantour massif being located at the transition between the Alps and the Mediterranean Sea, its deglaciation chronology can be compared to the sediment budget of the Var River marine delta. In this paper, the deglaciation is constrained by 13 new and 22 reassessed Cosmic-Ray Exposure (CRE) ^{10}Be datings of moraines and polished crystalline bedrocks. These data allow for the first time to fully reconstruct the deglaciation history at the scale of the entire massif, in agreement with a major glacier recession at ca. 15 ka, at the onset of Bølling transition. This contribution reveals a glacier–climate relationship more sensitive to warming phases in the southern Alps highlighted by a major decrease of

glaciers after ca. 15 ka. This major deglaciation is correlated with a 2.5 fold decrease of sediment discharge of rivers into the Mediterranean Sea. Main deglaciation of the massif upper slopes (2,700-2,800 m a.s.l.) occurred after the LGM at 20.8-18.6 ka, followed by the lower slopes (2,300 m a.s.l.) at 15.3-14.2 ka. Finally, the flat polished surfaces above 2,600 m a.s.l. and the zones confined within narrow lateral valleys were likely affected by progressive ice melting of remaining debris covered glaciers and moraine erosion following the Younger Dryas re-advance stage between 12 and 8-9 ka. At lower elevations, a sediment core in the Vens Lake located at 2,300 m a.s.l., shows onset of lake sedimentation at ca. 14 ka and a transition towards a vegetated environment after 8 ka. Final stabilization of moraines occurred at 5 ka, which might reflect denudation acceleration during the Holocene humid phase.

Key words: Landscape evolution / deglaciation / debris covered glaciers / Post-glacial erosion / ^{10}Be CRE dating

1. Introduction

The Mediterranean and Alpine regions respond differently to changing climate conditions mainly due to atmospheric circulation reorganization (e.g., Florineth and Schlüchter, 2000). In the Mediterranean region, the glacier–climate relationship is suggested to be more sensitive to fluctuations of the precipitation regimes (e.g., Hugues et al., 2006). However, the glacier extents and the chronology of the deglaciation on the SW Alps slopes is still a matter of debate (Darnault et al., 2012; Brisset et al., 2017; Federici et al., 2017), due to the lack of any preserved low-valley frontal moraines in the upper Tinée and Vésubie valleys on the French side. These data on glacial extent and timing of deglaciation are key for constraining inputs in source-to-sink approaches through the Var River system to the Ligurian (Mediterranean) sea that provide an ideal, relatively small watershed responsive to climate change (Bonneau et al.,

2014; 2017; Rolland et al., 2017). Notably, in their studies, Bonneau et al. (2014, 2017) and Rolland et al. (2017) estimated that the sediment fluxes through the Var routing system have increased by a factor ~2.5 during the Last Glacial Maximum (LGM) before dropping significantly to the current fluxes at 14-15 ka. Thus, Bonneau et al. (2017) proposed that glacial erosion remained high until the Gschnitz readvance at 15.7 ka, which they ascribe to the permanence of efficient glacial erosion well after the LGM. These data agree with very high incision rates, >10 mm yr^{-1} in the Upper Tinée Valley, until 14 ka (Rolland et al., 2017). However, it is still not possible to confirm that these high river sediment fluxes are related to glacial erosion as: (i) neither frontal moraine remains exist at low elevation in the valleys; (ii) nor complete deglaciation chronology of the Southern slope of the Argentera-Mercantour range is available.

Aiming to provide further constrains regarding the deglaciation chronology and the glacial erosion, this study focuses on the detailed analysis of the deglaciation chronology and moraine erosion within a zone where the last deglaciation chronology is well established by the sedimentological analysis of an Alpine lake (Petersen et al. 2014; Brisset et al. 2015). This is performed through the CRE dating of moraine boulders and polished surfaces. Moraines will be used as markers of the onset of deglaciation, while polished surfaces CRE ages will be used to infer the extent of ice on the upper slopes, and the abandonment of the bedrock by debris-covered glacier in the high valley floors. The relationships between the Alpine geomorphology and the deglaciation stages have been investigated through a new set of ^{10}Be CRE ages. These data were obtained from in-situ produced ^{10}Be concentrations measured in the quartz mineral fraction of polished glacial surfaces surrounding the Vens lakes in a high valley of the Argentera-Mercantour crystalline Massif in the SW French and Italian Alps.

2. Constraints on the post-LGM deglaciation

2.1. Deglaciation at the scale of the Alps & Mediterranean region

In the Alps, several studies have yielded a LGM age ranging from 20 to 30 ka (e.g., Cossart et al. 2010; Coutterand 2010; Wirsig et al. 2016). The LGM probably culminated around 21 ka in both the north and the south parts of the Alps (e.g., Jorda et al. 2000; Mix et al. 2001; see a review in Ivy-Ochs et al., 2009). The LGM stage is followed by at least two cold periods well expressed in the northern and eastern Alps: the Gschnitz readvance is dated at 17–16 ka (Maisch 1992; Ivy-Ochs et al. 2006a-b; 2008) and the Egesen stadial at 13.0–11.5 ka (Ivy-Ochs et al. 2009; Schindelwig et al. 2012). These two readvances may be attributed to the two most significant climatic deteriorations of Termination 1, the Heinrich event 1 at ~16.8 ka and the Younger Dryas at 12.9–11.5 ka (Bond et al. 1992; Böhlert et al. 2011; Clark et al. 2012; Wirsig et al. 2016). A similar chronology is confirmed in the Western Alps (e.g., Delunel 2010; Chenet et al. 2016), in the Pyrenees and Iberia (e.g., Rodriguez-Rodriguez et al. 2014; Palacios et al. 2017; Fernández-Fernández et al. 2017). In contrast, in the peri-Mediterranean settings, Hughes et al. (2006) suggested that the climatic conditions of Heinrich events promoted retreat or at least a stable glacier front, due to reduced precipitations. Around 10 ka, at the scale of the Alps and the Mediterranean region, glaciers had retreated to their Little Ice Age (LIA) extent or even more upstream (Ivy-Ochs et al. 2009; Solomina et al. 2015). However, the Younger Dryas period is followed by three late glaciation stages dated from 9.2 to 5.6 cal. ka BP, although these are not clearly evidenced in the SW Alps. They occurred between 9.2 and 8.2 cal. ka BP for the oldest one, between 7.4 and 6.6 cal. ka BP for the intermediate one, and between 6.2 and 5.6 cal. ka BP for the youngest one (Soldati et al. 2004; Nicolussi et al. 2005; Hormes et al. 2006; Kerschner et al. 2006; Joerin et al. 2008). Up to now, these late pulses of glacier extensions and recessions have been dated and documented in the central and northern Alps, essentially through dating

of moraines (e.g., Wirsig et al. 2016 and references therein), and the extension of these phases down to the SW Alps remains an open question.

2.2. Deglaciation in the Argentera-Mercantour massif (SW Alps)

Distinct glaciation and deglaciation patterns are suggested for the north and south slopes of the Argentera-Mercantour massif. On the northern (Italian) side of the Argentera massif, a sequence of moraines along the Gesso Valley (Fig. 1) allows to pinpoint the deglaciation history by ^{10}Be CRE dating of boulders (Federici et al. 2008, 2011, 2017; Tremblay et al., 2018): (1) The LGM is dated at 21-24 ka relying on a frontal moraine located 710-770 m a.s.l. (Federici et al. 2017, Tremblay et al., 2018); (2) the Bühl Stadial (~18.5 ka) is defined from moraine boulders at 820-880 m (Federici et al. 2017), while similar within error ages (16-19 ka) are obtained by Tremblay et al. (2018) from moraine boulders at 860 m; (3) the Egesen Stadial (12.0-13.9 ka) is defined by Federici et al. (2017) from moraine boulders at 1800 m, while Tremblay et al. (2018) obtained a slightly older age (14.1 ± 0.6 ka) at a similar elevation, which could relate this glacial phase to the onset of the Bølling transition (before the Older Dryas). Three undated early Holocene glacial stages are also identified by Federici et al. (2017), who proposed that they could correspond to the 11.4, 8.2 and 3 ka cold events.

On the southern side of the massif, these events are still not clearly identified, mainly due to the absence of any preserved frontal moraines at low elevation in the main valleys. The geomorphology of the high valleys is featured by polished glacier surfaces with a striking break in slopes. To the highest (the flatter ones) slopes are associated the oldest ^{10}Be CRE ages (18-22 ka), which highlight a first deglaciation phase (the presented ages are recalculated from Darnault et al. (2012) using updated ^{10}Be production rates, see suppl. Table 1). To the lower (the steeper ones) slopes are associated ^{10}Be CRE ages mainly in the ranges 14-15 ka and 9-11.5 ka, which agrees with glaciers re-advance at the transition between the Oldest and

Older Dryas and during the Younger Dryas cold period. In the Tinée Valley, CRE (^{10}Be and ^{36}Cl) dating at 20-14 ka and 11 ka of polished river gorges surfaces located at 1000 m a.s.l. and 2300 m a.s.l., respectively, constrain high fluvial incision, which may also be used as a proxy for increased erosion during glacial stages (Rolland et al., 2017; Fig. 2).

Up to now, it is still unclear if the revealed differences between the south and north slopes of the Argentera-Mercantour massif are only due to poor data coverage, or reflect a real difference in the slopes evolution. To solve this conundrum, we attempt in this work to complement and integrate the existing and new CRE dataset for both sides of the massif.

3. Study area

The study area is located in the Argentera-Mercantour massif (SW Alps) along the upper Tinée Valley (Figure 1) where climatic fluctuations, and in particular the chronology of glacier retreat since the LGM, have been investigated by several studies (Bigot-Cormier et al., 2005; Sanchez et al., 2010a; Darnault et al., 2012; Saillard et al., 2014; Brisset et al., 2015; Rolland et al., 2017).

3.1. Geography and geology of the study area

The study area lies in the Vens upper catchment (44.3°N; 6.95°E), whose elevations range from 2300 to 2980 m a.s.l. The main basement outcrop consists of crystalline rocks: granite and gneiss (Suppl. Mat. 1; 94% of the catchment). Permian–Triassic dolomites and sandstones (0.24 km^2; 6% of the catchment) are locally preserved on northeast-facing crests. The selected massif contains evidence of active tectonics through localized deformations in narrow fault corridors, some large landslides and recurrent seismic activity (Sanchez et al. 2010a-b; 2011; Darnault et al. 2012; Bauve et al. 2014). The mapped faults and related landslides occur in the lower Vens Valley and a fault segment also cross-cuts the upper Vens

Lake (Fig. 3, Suppl. Mat. 1). Such active faults might account for boulder instability and affect the CRE dating (e.g., Hugues et al., 2018).

3.2. Geomorphology of the study area

The Argentera-Mercantour massif, with several peaks above 3000 m a.s.l., is one of the highest massifs in the Western Alps. The Vens catchment is a glacial cirque located in the northwestern part of massif, on the left bank of the Tinée Valley (Fig. 2). Geomorphological analyses performed in the Vens Valley reveal the presence of several cirques and many well-preserved glacially polished rock surfaces and thick (5-15 m) blocky glacial sediments supporting that the origin of the sampled exposed surfaces is related to the valley's past glacial history (Figs. 4-6). The polished surfaces show smooth striated glacial steps (Fig. 4). Several coalescent cirques are recognized on the southern slopes, which correspond to glacier accumulation zones. From geomorphological observations, four glacial stages were recognized in the cirque between 2300 and 2800 m a.s.l. (Brisset et al. 2015). The most prominent glacial deposits on the glacial threshold at the lower mouth of the upper Vens Lake are attributed to the "Vens-I" Stage. A minimum age for the "Vens-I" stage is provided by ^{14}C dating of core sediments in the upper Vens lake combined with pollen biostratigraphy. These suggest a minimum deglaciation of the cirque catchments between 14,500 and 13,000 cal. BP, i.e., during the Late Glacial Interstadial (Greenland Interstadial-1e) (Brisset et al. 2015). Furthermore, three glacial stages are found upstream Lake Vens in the Terres Rousses River Valley, hereafter referred as "Vens-II" to "Vens-IV" following Brisset et al. (2015). However, these stages remain geochronologically unconstrained. The Vens lake core exhibits about 10 m of sediments deposited since ~14.5 ka cal. BP, with a first episode of deposition of glacier derived light-blue sediments at a high sedimentation rate of 0.15 $cm.yr^{-1}$and up to about 10 ka cal. BP , followed by a second episode taking place at a lower sedimentation rate of 0.04

cm.yr^{-1} at ~10-8 ka cal. BP, the sediments finally grading into a dark-brown diatom-rich clay (Brisset et al. 2015). This sedimentological change at 10-8 ka may be explained by a transition from a glacial to a non-glacial environment, or might be explained by the erosion of moraines.

4. Methodology and Analytical Procedures

4.1. Sampling strategy

To establish the chronology of the last major deglaciation phases, dating were performed using the CRE dating method based on the time-dependent accumulation of in-situ produced cosmogenic ^{10}Be, as detailed in Brown et al. (1991) and Siame et al. (2000) and reviewed in Gosse and Philips (2001). Aiming to constrain the last glaciation phases of the Upper Vens glaciers, we have sampled both moraine boulders and flat polished glacier-striated surfaces (Figure 4). The relevant data obtained on steep surfaces in the neighboring Fer Valley (Table 2) presented in Darnault et al. (2012) were reassessed for comparison using the more accurate and precise updated cosmogenic production rates.

Sampling has been performed in the upper part of the north-west oriented Vens tributary where glacially polished rock surfaces are numerous. The crystalline bedrock is suited for measurements of the in situ-produced ^{10}Be concentrations accumulated in their quartz mineral fraction (Fig. 4, Suppl. Mat. 1).

Two distinct areas have been targeted in the Vens Valley:

- The upper part of the Vens Valley (Fourchas Lake area), which lies between 2450 and 2982 m a.s.l. elevation. The orientation of this part of the valley, on the northern side behind a crestline, makes it a cold and shaded zone, especially in winter times. In this zone, the latest glacial features, including active debris covered glaciers, are preserved.

- The lower part surrounding the Vens lakes (Vens Lake area) located between two rock bars lies between 2350 m and 2450 m a.s.l. elevation. The orientation of this part of the valley is east-west. The northern side of the lake is a south face significantly more exposed to sunlight than the high valley Fourchas Lake area. This area corresponds to the influence zone of the "Vens-I" glacial stage.

We focused our sampling on "Vens-I" and "Vens-II" for this study, as the later stages ("Vens-III-IV") not only are of small amplitude but also may have not been exposed to cosmic-rays long enough (<1000 years) to allow accurate and precise CRE dating. Furthermore, for the dating of "Vens-I" stage, polished surfaces were sampled close to the lake as well as higher up along the slopes on both sides to evaluate the possible shielding effects of moraines dating. As all the fine-grained (<1 cm) moraine material was removed by erosion, this precludes evaluating the original thickness and lateral extent of moraines. For the dating of the "Vens-II" episode, sampling was undertaken on the mainstream upper valley (Fourchas Lake area), below the height of lateral moraines along the Terres Rousses River. Sampling was undertaken at different elevations along the stream.

Frontal moraine boulders have been sampled in the lower Vens Lake area to provide a minimum Vens-I deglaciation age. We sampled the moraines in winter to select blocks that were not covered by thick snow in winter time and so prevent corrections due to snow shielding. Three moraine boulders were sampled in early April 2018 (Fig. 4), when the massif was covered by a thick snow blanket. In addition, ten surfaces from quartz veins or gneisses have been collected between 2350 and 2600 m a.s.l. in the upper part of the Vens glacier-incised valley (Fig. 5). All well-preserved surfaces exhibit clear glacial striae, which is consistent with low denudation rates and is well-suited for ^{10}Be CRE dating (see following section 'Analytical Procedures') or preservation below glacial till. The ^{10}Be CRE ages calculated for these surfaces are assumed to correspond either to the main

glacier retreat events, or to the denudation rates of the moraines at the sampling sites. Moreover, Darnault et al. (2012) study provides ^{10}Be CRE data in the neighbouring south-west striking Fer Valley (Fig. 2). However, in contrast to Darnault et al. (2012) who sampled vertical scarps, we targeted basement polished surfaces in order to compare these ages to the moraine ages, evaluate the duration of moraine erosion and estimate the moment of their stabilization on the valley floor. Basement polished surfaces are thus mostly covered by snow during winter time due to the flat lying basement, except for sample Clap 51 which was sampled in a steep rock scarp (Fig. 4).

4.2. In-situ produced ^{10}Be dating method.

The physico-chemical treatment of the samples as well as the Acceleration Mass Spectrometry (AMS) measurements of the Be isotopic ratios were carried out at the "Laboratoire National des Nucléides Cosmogéniques (LN2C)" ("National Laboratory of Cosmogenic Nuclides", CEREGE, Aix-en-Provence). Samples were prepared for ^{10}Be measurements following procedures adapted from Brown et al. (1991) and Merchel and Herpers (1999). Crushed rocks were sieved and magnetic grains were discarded using a magnetic separator. Pure quartz was obtained from the non-magnetic 250-800 µm fraction by repeated H_2SiF_6 - HCl etching. Atmospheric ^{10}Be was subsequently eliminated by sequential dissolutions with diluted HF. After addition in each sample of ~100 µl of an in-house 3.10^{-3} g/g ^{9}Be carrier solution prepared from deep-mined phenakite (Merchel et al., 2008), residual grains (the isolated and purified quartz fraction) were dissolved in a concentrated HF solution. After converting the dissolved material from a fluoride form to a chloride form, the beryllium was separated from the obtained solution using ion exchange resin (DOWEX 1X8 100-200 mesh then DOWEX 50WX8 100-200 mesh) as described in Merchel and Herpers (1999). Finally, alkaline precipitations allowed to extract pure Be oxy-hydroxydes that are oxidized

by heating at 800°C during 1 hour. BeO targets were prepared for measurement at the French National Accelerator Mass Spectrometry facility, ASTER, located at CEREGE in Aix-en-Provence. The measured $^{10}Be/^{9}Be$ ratios were corrected for procedural blanks and calibrated against the National Institute of Standards and Technology standard reference material 4325 by using an assigned value of 2.79 ± 0.03 x 10^{-11} and using a ^{10}Be half-life of (1.387 ± 0.012) x10^{6} years (Korschinek et al. 2010; Chmeleff et al., 2010). The presented ages were calculated from the measured concentrations according to the procedures proposed by Sanchez et al. (2010a) and Darnault et al. (2012) and thus using the following equation:

$$C_{(\chi,\varepsilon,t)} = C_0.e^{-\lambda t} + \frac{P_{spal.}}{\lambda}.e^{-\frac{\chi}{\Lambda_n}}\left[1-e^{-t\lambda}\right] + \frac{P_{\mu s}}{\lambda}.e^{-\frac{\chi}{\Lambda_{\mu s}}}\left[1-e^{-t\lambda}\right] + \frac{P_{\mu f}}{\lambda}.e^{-\frac{\chi}{\Lambda_{\mu f}}}\left[1-e^{-t\lambda}\right]$$

where $C_{(\chi,\varepsilon,t)}$ is the ^{10}Be concentration as a function of depth χ (g.cm^{-2}), erosion ε (g.cm^{-2}.yr^{-1}) and t the exposure time (year); C_0 is the ^{10}Be inherited concentration prior to exposure at the surface. Λ_n, $\Lambda_{\mu s}$ and $\Lambda_{\mu f}$ are the effective apparent attenuation length (g cm^{-2}) for neutrons, slow muons and fast muons, respectively. P_{spal}, $P_{\mu s}$ and $P_{\mu f}$ are the relative spallogenic, slow and fast muons production rates. All calculations were performed using attenuation lengths of 160, 1500 and 4320 g cm^{-2} for neutrons, slow muons and fast muons, respectively. These values are based on field-calibrated measurements (Braucher et al., 2011). Muons contributions of 0.012 and 0.04 at g^{-1} yr^{-1} at sea level (Braucher et al., 2011) have been scaled for altitude only using attenuations lengths of 260 and 510 g cm^{-2} in the atmosphere for slow and fast muons, respectively. A modern spallogenic production rate at sea-level and high latitude of 4.02 ± 0.2 at g^{-1} yr^{-1} computed for internal consistency from the data of Stone (2000) according to the conclusions of the published study on absolute calibration of ^{10}Be AMS standards (Nishiizumi et al., 2007), was used. This sea-level and high latitude production rate has then been scaled for the sampling altitudes and latitudes using the scaling factors proposed by Stone (2000). The surface production rates were corrected for local slope

and topographic shielding due to surrounding morphologies following Dunne et al. (1999). Snow shielding corrections may increase the calculated ^{10}Be ages by up to 25% assuming a reasonable snow height of 1.5 m in Fourchas Lake area, 0.5 m in Vens Lake area, during 6 months (Table 1), the snow density (ρ) being 0.3 g.cm^{-3} (Hippolyte et al., 2006; Delunel et al., 2014). This is a relatively small correction considering the overall uncertainties associated to the age calculation, but has to be taken into account, except for samples for which we checked that they remained out of the snow during winter time due to local configuration. Corrections include the analytical uncertainties (reported as 1σ) estimated using a conservative 0.5% external machine uncertainty (Arnold et al. 2010), 1.08% uncertainty on the certified standard ratio, a 1σ uncertainty associated to the mean of the standard ratio measurements during the measurement cycles, 1σ statistical error on counted ^{10}Be events, and the uncertainty associated with the chemical and analytical blank correction (associated ^{10}Be/^{9}Be blank ratio was 3.5 $10^{-15} \pm 2\ 10^{-16}$). In the following, we will refer to ages as ^{10}Be CRE ages. The overall uncertainties associated to the presented ^{10}Be CRE ages also propagate an additional ~5% uncertainty linked to the production rate determination. Moreover, considering the observed preservation of striation on the glacier polished surfaces, all ^{10}Be ages were calculated considering denudation rate as negligible during the time period involved, and are thus minimum ages.

5. ^{10}Be CRE dating results

5.1. Moraine blocks

The dated moraine is a lateral to frontal "Vens-I" moraine system. It covers the tip of a flat valley part at the mouth of upper Vens Lake and turns along the valley slopes in a crescent-like morphology (Figs. 5-6). The selected moraine blocks consist of unsorted boulders of variable sizes (maximum diameter of 2 m) accumulated above the polished rock surface on

the glacial threshold, at the lower mouth of the main Vens Lake (2300 m a.s.l.). ^{10}Be CRE ages obtained on these moraine boulders are clustered at 14.2 ± 0.4 – 15.2 ± 0.6 ka (Table 1), which constrains the main "Vens-I" deglaciation stage.

5.2. Polished bedrock surfaces

Accordingly, the calculated ^{10}Be CRE ages of polished glacial surfaces are younger than the frontal moraine. They range from ~2.9 to 14.7 ka (snow corrected, Table 1, Figs. 4-5). Two areas are distinguishable based on the ages repartition : (i) in the upper part of the valley (Fourchas Lake area), on average, the ^{10}Be CRE ages are slightly older and more clustered than (ii) those acquired around the Vens lakes (Vens Lake area; Figure 7B,C).

(i) **Fourchas Lake area**: Five samples (Clap 57, 62, 63, 66, 67) yield an average CRE age of 7.4 ± 1.2 ka (1σ). However, the slightly younger CRE age of sample Clap 57 (6.3 ± 0.4 ka), which may be due to the shielding by a former (and now eroded) moraine till (see section 5.2), is considered as an outlier and discarded. As these samples were not collected in vertical scarps, a supplementary correction linked to potential snow cover is required. Following Delunel et al. (2014), a snow density of 0.3 associated with a thickness of 150 cm during the winter months (December-May, Table 1) slightly increase the Fourchas Lake area average CRE age to 9.8 ± 1.7 ka (Figure 7B). The $\chi^2_{,95}$ test performed on the CRE ages acquired in Fourchas Lake area indicates that they all belong to the same population which allows ascribing a minimum CRE age for the final melting of the "Vens-II" rock-glacier at ~9.8 ± 1.7 ka in this part of the valley.

(ii) **Vens Lake area**: Four samples (Clap 52, 54, 56, 58) yield an average age of 5.3 ± 2.4 ka (Table 1, Figs. 5 and 7C), with a maximum age (Clap 51) of 14.7 ± 1.0 ka. The $\chi^2_{,95}$ test performed on the CRE ages acquired in Vens Lake area indicates that they

are highly dispersed (Figure 7C), do not statistically belong to the same population, and thus do not, as a whole, allow assigning a minimum CRE age to the glacier retreat. Their distribution most likely results from the occurrence of local post-glacial events. As the age of 14.7 ± 1.0 ka is similar to the moraine block ages, it confirms that "Vens-I" deglaciation occurred within the range 14.2– 15.2 ka.

5.3. Geomorphological evolution

After the major "Vens-I" deglaciation, represented by the frontal moraine dated in section 5.1, further three glacial stages are evidenced above Lake Vens in the Fourchas Lake area (Figs. 5-6). "Vens-II" stage is represented by a poorly preserved recessional moraine positioned closed to the valley floor in a lateral position relative to glacier flow at an altitude of 2400 m a.s.l. A glacially polished surface is nicely exposed all along the Terres Rousses River and Fourchas Lake area. These observations suggest an extent of "Vens-II" over the whole high valley. The lack of well-preserved "Vens-II" frontal moraine suggests a maximal extent for this phase probably down to Vens Lakes and a retreat in the whole cirque marked by a stage of debris-covered glacier during which no frontal moraine was formed, or may have been eroded. Large areas are covered with blocky material, which suggests the presence of such a debris-covered glacier (Fig. 6). The fact that ages clustered at 9.8 ± 1.7 ka were obtained on flat polished surfaces around Fourchas Lake is in good agreement with a 'Vens-II' glacial event preserved in the high valley where a debris covered glacier was maintained, as featured by numerous block remains on the valley floor (Fig. 6). It is also possible that the landforms mapped as "Vens III" and "IV" formed and moved into the area to form this debris covered glacier during the Younger Dryas, after the upper valley was totally freed from its ice during the "Vens I" melting stage. It has to be noticed that a decreasing pattern in ages can be seen from below the Fourchas Lake towards the highest sample, indicating a progressive recession of

the debris covered glacier. There, the oldest age, taking into account the snow cover, is of 12.2 ± 0.7 ka (Clap 62), which corresponds to the Younger Dryas. The CRE ages upstream Fourchas Lake decrease from the Clap 62 sample located at 2508 m to the Clap 63 sample located at 2599 m (Figure 5), which may indicate a progressive regression (within 2.5 ka) of glacier to the upper and shadiest zone of the valley until ~ 8ka. Based on this age pattern, we interpret the "Vens-II" features as representing the glacial recession following the Younger Dryas.

The highest ridges of "Vens-III" and "Vens-IV" stages, at altitudes of 2600 m and 2700 m, respectively, are small-amplitude end-moraines, positioned transversally to glacier flow on both NE and SW flanks of the valley. "Vens-III" and "IV" are well preserved below Claï Supérieur Peak on the left bank of the valley, where they form two distinct moraines, while similar glacier features are less discernible in the eastern right part of the glacial cirque. There, the end-moraines of "Vens-III" and "IV" are undifferentiated. In the valley higher part, to its southeast end, there is still evidence of a rock-glacier near to the Equilibrium Line Altitude as in other parts of the massif (Ribolini et al. 2007; Brisset et al. 2015; Fig. 6).

6. Discussion

An increasing number of studies have been conducted in order to better understand climatic fluctuations during the transition between the end of the glacial period (or 'Late-glacial period'), which followed the LGM and the beginning of the subsequent interglacial period (Holocene). These studies are based on lake sediment analysis (e.g., Leemann and Niessen 1994; Brisset et al., 2015), radiocarbon dating of organic remains (e.g., Hormes et al. 2001; Joerin et al. 2006) and surface exposure ages using Cosmic-Ray Exposure (CRE) dating of moraines and polished basement rocks (e.g., Kelly et al. 2001; 2006; Ivy-Ochs et al. 2006a-b;

Darnault et al. 2012; Schimmelpfennig et al. 2012; Wirsig et al. 2016). These works allow providing constraints on recent Quaternary climate changes and subsequent geological hazards such as landslides (e.g., Sanchez et al. 2010a; Ballantyne et al. 2014; Zérathe et al. 2014). However, the significance of CRE ages with respect to glacier abandonment in a given area has to be addressed with respect to several processes comprising glacier melting and subsequent moraine reorganization and denudation, the development of screes and soils, and the gravitational destabilizations (e.g., Cossart et al. 2010; Hippolyte et al. 2009; Chenet et al. 2016). These latter processes may significantly affect the CRE dating as they lead to lowering the exposure age of bedrock surfaces, which may critically change a given interpretation of glacier melting and abandonment. The results of this study provide new ^{10}Be CRE ages interpreted in light of glacier recession and subsequent interglacial processes, which may include: (i) major glacier recession phases since the LGM; (ii) formation of a debris covered glacier; (iii) moraine denudation dynamics; and, (iv) emplacement of soils or screes. Most CRE ages obtained from the Vens Valley polished bedrock surfaces are younger than expected. Several hypotheses expressed in the following parts (6.1 and 6.2) can be proposed to explain the results presented in this work: (1) preservation of a debris covered glacier in the upper Vens Valley; and, (2) dynamics of moraine denudation. In the following discussion, we compare the CRE results with those of polished rock scarps in neighboring valleys, and with the Vens Lake sedimentary record.

6.1. Permanence of debris covered glaciers after the Younger Dryas deglaciation phase

The dating of Fourchas Lake area polished surfaces yields an age of ca. 9.8 ± 1.7 ka, with a regression along the N facing upper valley until ~ 8 ka as well as geomorphologic observations (section 5.3) suggest that a "Vens-II" glacial event is preserved in the high valley where a debris covered glacier was maintained. During the course of deglaciation,

glaciers indeed commonly evolve into debris covered glaciers (Giardino et al., 1987; Rau et al. 2005; Monnier and Kinnard 2015). The dynamics and evolution of these debris covered glaciers are clearly different from those of "white" glaciers, which present a rock-free surface (e.g., Giardino et al., 1987). In the debris covered glaciers, the ice is preserved for a long time as it is insulated from heating by the rock layer. Consequently, the glacier is maintained in the higher cirque and is nearly immobile. It is well known from other Alpine massifs at similar elevations (Ecrins-Pelvoux, Mont Blanc, Vanoise and Mont Blanc ranges, for instance) that debris covered glaciers were maintained in north-facing valleys until the present day down to elevations as low as ~1700 m for the Miage Glacier in Val Veni, Italy (Deline 1999; Akçar et al. 2012; Fig. 1A), or ~1900 m for the 'Glacier Noir' in Les Ecrins, France (Figs. 1A and 8). If these massifs have preserved significant volumes of debris covered glaciers until the present-day, it is likely that similar glaciers may have existed also in the Argentera-Mercantour massif. Actually, the upper Vens Valley's Fourchas Lake area still preserves some very small debris covered glaciers (Figs. 5-6).

The geomorphology of the Vens Valley may be one of the causes allowing the preservation of a debris covered glacier invoked as a potential explanation for the relatively young CRE ages obtained in this valley:

- Larger and flatter than neighbouring valleys, the surface of the Vens Valley watershed is roughly 10 km^2 (Figure 3). This may lead to a stagnation of the ice mass, and to a significantly higher inertia of glacier melting at that elevation. For instance, the size, slope, orientation and altitude of this high valley is similar to those of the 'Glacier Noir' in Les Ecrins massif, some 30 km away to the NW (Figs. 1 and 8), which remained glaciated and relatively stagnant until the present-day. The Vens Valley only differs from the latter by the altitude (500 m less) of the north-facing scarps dominating the valley.

- The north westerly orientation of the Vens Valley upper part, associated to high crests and summits, implies a reduced exposure of the snow accumulation area (or cirque) to the sun. This should have also slowed the melting of ice. One of the main current observations confirming this hypothesis is the persistence of a rock-glacier in the upper valley part (Figs. 3B, 6), which is rare in the whole Argentera-Mercantour massif.

6.2. Potential causes of young ^{10}Be CRE ages around Vens lakes (Vens Lake area)

Several causes leading to the observed scattered, and especially younger, CRE ages could be invoked: (i) the development of soils that would have been eroded afterwards; (ii) shielding by screes; and, (iii) the progressive denudation of the moraines by erosion that will free the polished surfaces. These causes are discussed here:

(i) The development of soils at a given stage of slope evolution may result in younger apparent ^{10}Be CRE ages, as suggested by the development and subsequent vanishing of soils in some Alpine valleys (Mourier et al. 2010; Giguet-Covex et al. 2011). To discuss this hypothesis, the thicknesses of soil required to 'apparent' exposure durations of 15 ka, 11 ka and 8 ka from the measured ^{10}Be CRE ages have been evaluated (Fig. 9). Table 2 presents the results obtained for each sample assuming a soil density of 2.0, according to Schalgenhauf et al. (2010). To obtain the measured ^{10}Be CRE ages from the chosen exposure durations, soil thicknesses ranging from 50 to 80 centimetres had to develop before being removed. However, soil formation is indeed thought to be a progressive process encompassing the whole Holocene (Egli et al. 2001; 2003). Moreover, the gneissic composition of the bedrock in this part of the massif does not allow an alteration rate of the substratum high enough to develop such a thick column of soil during this period of time (Egli et al. 2001).

(ii) The slope geomorphological features are not in agreement with a shielding effect due to screes. Because of the limited height of the upper slope rock scarp, the screes develop only in the upper half of the slope, while the presence of large and scattered erratic blocks argue for a former moraine remaining at the base of slope, that is at the mouth of the lake (Fig. 5).

(iii) Consequently, a shielding by residual till seems more likely. The progressive denudation of the moraines by runoff water will progressively free the big boulders and lead to the exposure of formerly polished surfaces. This moraine denudation process can be currently observed in other Alpine massifs (Fig. 8B). As moraine denudation leads to a diachronous exhumation of the bedrock surface, it can be hypothesized that the time interval between 14.7 and 2.9 ka corresponds to the time period necessary for a complete moraine denudation and stabilization. Age clustering around 5 ka might reflect erosion acceleration during the Holocene humid phase, which is well expressed in the ^{36}Cl dating record of river incision in the low valleys (Saillard et al. 2014; Rolland et al. 2017), and by onset of accelerated sedimentation rates recorded in the Vens sediments (Fig. 10; Brisset et al. 2015).

6.3. Comparison of CRE ages with the Vens lakes sediment record (Vens Lake area)

Mapping of geomorphic features around the lake evidences the presence of large erratic boulders that form the remains of a frontal-lateral moraine (Figs. 5-6). The glacier retreat at > ca. 14 ka is reflected by sedimentological changes in a proglacial lake as well as by the establishment of vegetation reflected by lacustrine pollen records (Brisset et al. 2015). The Vens Lake sediment is rich in magnetic minerals from the gneissic bedrock, especially in the bottom part of the sediment core. In the lake, between ~14 and ~10 ka, the lithotype consisting of fine to medium size blue-beige silts with maximal sedimentation rates (0.14 cm.yr^{-1}) is characteristic of a depositional environment in the distal position of a proglacial lake, or to the erosion of moraines ("glacial milk": glacier derived light-blue sediments,

Brisset et al. 2015; Fig. 10). Therefore, the large spread of ^{10}Be CRE ages around the lake is ascribed to the moraine erosion which mainly took place between 14 and 8 ka. At 8 ka, the sedimentation rate dropped to <0.04 cm.yr^{-1}, and the nature of the sediment became darker, and rich in clay and organic matter (Brisset et al., 2015). Palynological study reveals a trend towards a forest environment around the lake in this time range (Brisset et al., 2015). Therefore, the detailed analysis of the Vens lake sediment core concurs with the CRE dating of moraines and polished surfaces of Vens Lake area to constrain the age of bottom lake sediment formation at the Allerød, before 14,000 cal. BP. Considering the age of 15.3 ± 0.5 ka obtained in the lower part of the valley (Lake Vens region), age of the oldest moraine block (see the results section), the ^{10}Be CRE dating obtained in this study significantly extend the dating of the glacier recession in the Upper Vens Valley cirque (Fourchas Lake area).

6.4. Synthesis of the glacier retreat and moraine denudation in the upper part of the Mercantour range

For comparison, the 22 ^{10}Be CRE ages obtained by Darnault et al. (2012) on polished basement surfaces from the Fer and Rabuons valleys, which stand directly SE of the Vens Lakes area on the Southern flank of Tenibre Peak, were recalculated using the updated in situ ^{10}Be production rates (Figs. 2, 11; Table 3). These reassessed ages are in agreement with: (1) the deglaciation following the LGM of the upper slopes part at 18-22 ka; (2) a second phase of deglaciation corresponding to the "Vens-I" stage (14-15 ka, Fig. 11D) and to the Bølling transition (Oldest to Older Dryas); (3) the deglaciation of the lower slope part and of the fault zone corridor likely reflecting a late deglaciation and moraine erosion phase, which followed the Younger Dryas (9-11.5 ka). Several younger ages may be interpreted as resulting from some further erosion of glacial sediments at the foot of the slope and from gravitational destabilization in the fault zone (e.g., Hugues et al., 2018) until between 6 and 3 ka.

According to the presented CRE dating results on the southern slope of Argentera-Mercantour massif, and to studies in neighboring areas, including on the northern (Italian) slope of Argentera (see section 2), a synthesis of ages at the scale of the massif and a hypothetical reconstruction of the deglaciation in the Vens Valley is proposed in Figs. 12-13.

(A) Cosmogenic dating of frontal moraines at low elevation in the main valley on the north side of the Argentera – Mercantour evidence onset of LGM deglaciation at 21-24 ka at ~730 m (Federici et al. 2017, Tremblay et al., 2018), followed by a Bühl Stadial (~18.5 ka) glacier retreat at ~860 m (Federici et al. 2017; Tremblay et al., 2018; Fig. 12). These ages agree with the upper slope basement ^{10}Be CRE ages of 18-22 ka obtained on the southern slope of Tenibre (see previous section), which shows that the high altitude south facing slopes were freed of ice during this time range. Subsequent installation of modern denudation and fluvial incision in low valleys is also constrained at that time period by CRE dating of polished river surfaces, which highlight onset of fluvial erosion at 19-22 ka, and transient erosional events involving incision rates >10 mm.yr^{-1} at ~14 and ~11 ka (Saillard et al. 2014; Rolland et al. 2017, Petit et al., 2017).

(B) A second major phase of deglaciation ("Vens-I" phase) occurred in the high valleys at ~14 ka, at the transition between the Oldest and Older Dryas, and may be related to the onset of Bølling transition. On the south slope of the massif, the "Vens-I" moraines (2300 m a.s.l.) are dated at 15.3-14.2 ka, while on the northern slope, ages of ~14 ka are obtained at 1800m. Thus, an altitude difference of 500 m can be observed for the frontal moraines of this phase between the two sides of the massif.

(C) The main last phase of deglaciation ("Vens-II" phase) ranges between 9 and 11.5 ka (Fig. 11C). This phase coincides with the "Vens-II" moraines and debris covered glaciers confined to the highest and shadiest zones of the southern slopes (Vens

Fourchas Lake area). Other studies performed in the Alps lead to mean ages of 11-12 ka for deglaciation at the end of the Younger Dryas (Ivy-Ochs et al., 2009, and references therein). However, some more restricted glacier retreat phases are recognized after the Younger Dryas throughout the Alps (Kelly et al. 2001; Kerschner et al. 2006; Joerin et al. 2008; Darnault et al. 2012). The results presented here are in agreement with these observations, which argue for the preservation of small debris covered glaciers in shadiest and most elevated zones, well after the end of the Younger Dryas. In the upper Vens Valley, the local north westerly orientation and reduced sunlight exposure due to the high crests, associated to the relatively large watershed at an altitude >2300 m a.s.l., likely implies sufficient inertia for the glacially-derived "Vens-II-III" debris covered glaciers to finally melt entirely only at 9-10 ka (Figures 13B-C). Afterwards, progressive denudation of moraine remains until their final stabilization by soils at ca.2-4 ka leads to the progressive exposure of polished surfaces around the Vens lakes (Fig. 13D). Finally, the upper "Vens-IV" moraines may date back to the Little Ice Age, as proposed by Federici et al. (2017) for the upper moraines on the northern side of the massif.

7. Conclusion

This paper highlights how the dating of several types of geomorphologic features can be undertaken to reconstruct the phases of glacier abandonment and moraine erosion in a high-altitude environment. ^{10}Be CRE dating of flat and steep glacially polished glacial surfaces are combined to those of moraine blocks at the scale of the Argentera-Mercantour massif (SW Alps). These data allow reconstructing the glacial recessions and landscape evolution since the LGM. CRE ages obtained on steep glacially polished bedrock from the summit zone cluster at 18-22 ka, which highlights onset of LGM deglaciation in agreement with lower

valley frontal moraines on the Italian side. At elevations of 2300-2400 m (Vens Lake area), a dispersed distribution of ^{10}Be CRE ages is ascribed to post-deglacial denudation and moraine reorganization. Moraine block ages of 14.2-15.3 ka and maximum polished basement age of 14.7 ± 1.0 ka are interpreted as a minimum age for the main "Vens-I" glacier melting stage in the lower Vens valley, and as the onset of Alpine lakes formation and sedimentation at this altitude. These data show a major glacier recession during the Bølling transition, between the Oldest and Older Dryas, in agreement with deglaciation at the scale of the Alps. This major deglaciation is correlated to a 2.5-fold decrease in sediment fluxes documented in the Var River marine delta, after ca. ~15 ka. The final deglaciation in the upper valleys at elevations > 2400 m occurred after the Younger Dryas until ca. 9 ka, due to the permanence of debris covered glaciers in shadiest zones, as is currently observed in other high Alpine massifs. This phase of Early Holocene glacier melting is highlighted in the bottom of the Vens sediment cores exhibiting glacier derived light-blue sediments. The younger polished basement ^{10}Be CRE age clustering around 5 ka dates the final moraine stabilization stages, which might result from erosion acceleration during the Holocene humid phase.

Acknowledgements

This work benefited from support by the Observatoire de la Côte d'Azur (OCA). The ^{10}Be measurements were performed at the ASTER AMS national facility (CEREGE, Aix-en-Provence), which is supported by the INSU/CNRS, the ANR through the "Projets thématiques d'excellence" program for the "Equipements d'excellence" ASTER-CEREGE action and IRD. We wish to thank L. Léanni and F. Chauvet for their help during chemistry and measurements at CEREGE. We thank Fabien Arnaud, Elodie Brisset, Etienne Cossart, Bruno Wilhelm, Swann Zérathe, Ph. Deline and V. Rinterknecht for fruitful and stimulating discussions. We warmly thank the help of two anonymous reviewers and editors, which

significantly improved the former version of this manuscript, and G. Duclaux and G. Nolet for reviewing the English language.

References

Akçar N, Deline P, Ivy-Ochs S, Alfimov V, Hajdas I, Kubik PW, et al. 2012. The AD 1717 rock avalanche deposits in the upper Ferret Valley Italy): a dating approach with cosmogenic ^{10}Be. *Journal of Quaternary Science* **27** (4): 383-392.

Arnold M, Merchel S, Bourlès DL, Braucher, R., et al. 2010. The French accelerator mass spectrometry facility ASTER: Improved performance and developments. *Nucl. Instr. and Meth. in Phys. Res.* **B 268**: 1954–1959. Doi: 10.1016/j.nimb.2010.02.107.

Ballantyne CK, Sandeman GF, Stone JO, Wilson P. 2014. Rock-slope failure following Late Pleistocene deglaciation on tectonically stable mountainous terrain. *Quaternary Science Reviews* **86**: 144-157.

Bauve V, Plateaux R, Rolland Y, Sanchez G, Bethoux N, Delouis B, Darnault R. 2014. Long-lasting transcurrent tectonics in SW Alps evidenced by Neogene to present-day stress fields. *Tectonophysics,* doi:10.1016/j.tecto.2014.02.006.

Bigot-Cormier F, Braucher R, Bourlès D, Guglielmi Y, Dubar M, Stéphan JF. 2005. Chronological constraints on processes leading to large active landslides. *Earth and Planetary Science Letters* **235**: 141-150.

Böhlert R, Egli M, Maisch M, Brandová D, Ivy-Ochs S, Kubik PW, Haeberli W. 2011. Application of a combination of dating techniques to reconstruct the Lateglacial and early Holocene landscape history of the Albula region eastern Switzerland. *Geomorphology* **127**: 1-13.

Bond G, Heinrich H, Broecker W, et al. 1992. Evidence for massive discharge of icebergs into the North Atlantic Ocean during the last glacial period. *Nature* **360**: 245–249.

Bonneau L, Jorry SJ, Toucanne S., Silva Jacinto R, Emmanuel L. 2014. Millennial-scale response of a western Mediterranean river to late Quaternary climate changes: a view from the deep sea. *The Journal of Geology* **122(6)**: 687-703.

Bonneau L, Toucanne S, Bayon G, Jorry SJ, Emmanuel L, Jacinto RS. 2017. Glacial erosion dynamics in a small mountainous watershed (Southern French Alps): A source-to-sink approach. *Earth and Planetary Science Letters* **458** 366-379.

Bouissou S, Darnault R, Chemenda A, Rolland Y. 2012. Evolution of gravity-driven rock slope failure and associated fracturing: Geological analysis and numerical modelling. *Tectonophysics* **526–529**: 157-166.

Braucher R, Merchel S, Borgomano J, Bourlès DL. 2011. Production of cosmogenic radionuclides at great depth: a multi element approach. *Earth and Planetary Science Letters* **309**: 1-9.

Brisset E, Guiter F, Miramont C, Revel M, Anthony E.J, Delhon C, Arnaud F, Malet E, de Beaulieu J.-L. 2015. Lateglacial/Holocene environmental changes in the Mediterranean Alps inferred from lacustrine sediments. *Quaternary Science Reviews* **110**: 49-71. doi: 10.1016/j.quascirev.2014.12.004.

Brown ET, Edmond JM, Raisbeck GM, Yiou F, Kurz MD, Brook EJ, 1991. Examination of surface exposure ages of Antarctic moraines using in situ produces ^{10}Be and ^{26}Al. *Geochimica et Cosmochimica Acta* **55**: 2269-2283.

Chenet M, Brunstein D, Jomelli V, Roussel E, Rinterknecht V, Mokadem F, ASTER Team. 2016. ^{10}Be cosmic-ray exposure dating of moraines and rock avalanches in the Upper

Romanche valley French Alps): Evidence of two glacial advances during the Late Glacial/Holocene transition. *Quaternary Science Reviews* **148**: 209-221.

Clark PU, Shakun JD, Baker PA, et al. 2012. Global climate evolution during the last deglaciation, *Proceedings of the National Academy of Sciences of the United States of America* **109**: E1134–E1142.

Chmeleff J, Von Blanckenburg F, Kossert K, Jakob D, 2010. Determination of the ^{10}Be half-life by multicollector ICP-MS and liquid scintillation counting. *Nuclear Instrument and Methods in Physics Research B* **268**: 192-199.

Cossart E, Fort M, Bourlès D, Carcaillet J, Perrier R, Siame L, Braucher R. 2010. Climatic significance of glacier retreat and rockglaciers re-assessed in the light of cosmogenic dating and weathering rind thickness in Clarée Valley Briançonnais French Alps. *Catena* **80**: 204-219.

Coutterand S. 2010. Etude géomorphologique des flux glaciaires dans les Alpes Nord-Occidentales au Pléistocène récent, Du maximum de la dernière glaciation aux premières étapes de la déglaciation. PhD Thesis, university of Chambéry.

Darnault R. 2012. Étude de l'évolution des versants de montagne et des déstabilisations gravitaires associées par une approche couplée d'observations sismotectoniques, de datations géochronologiques et de modélisations PhD Thesis, university of Nice Sophia Antipolis.

Darnault R, Rolland Y, Braucher R, Bourlès D, Revel M, Sanchez G, Bouissou S. 2012. Timing of the last deglaciation revealed by receding glaciers at the Alpine-scale: impact on mountain geomorphology. *Quaternary Science Reviews* **31**: 127-142.

Deline P. 1999. Late Holocene fluctuations of the Miage glacier Val Veny Valley of Aosta. *Quaternaire* **10(1)**: 5-13.

Delunel R. 2010. Evolution géomorphologique du massif des Ecrins-Pelvoux depuis le Dernier Maximum Glaciaire–Apports des nucléides cosmogéniques produits in-situ. ph.D. Université Joseph-Fourier-Grenoble I.

Delunel R, Bourles DL, van der Beek P, Schlunegger F, Leya I, Masarik J, Paquet E. 2014. Snow shielding factors for cosmogenic nuclide dating inferred from long-term neutron detector monitoring. *Quaternary Geochronology* **24:** 16-26.

Dunne J, Elmore D, Muzikar P. 1999. Scaling factors for the rates of production of cosmogenic nuclides for geometric shielding and attenuation at depth on sloped surfaces. *Geomorphology* **27**: 3-11.

Egli M, Mirabella A, Fitze P. 2001. Weathering and evolution of soils formed on granitic glacial deposits: results from chronosequences of Swiss alpine environments. *Catena* **45:** 19–47.

Egli M, Mirabella A, Fitze P. 2003. Formation rates of smectites derived from two Holocene chronosequences in the Swiss Alps. *Geoderma* **117**: 81-98.

Federici PR, Granger D, E, Pappalardo M, Ribolini A, Spagnolo M, Cyr AJ. 2008. Exposure age dating and Equilibrium Line Altitude reconstruction of an Egesen moraine in the Maritime Alps Italy. *Boreas* **37**: 245-253.

Federici PR, Granger DE, Ribolini A, Spagnolo M, Pappalardo M, Cyr AJ. 2011. Last Glacial Maximum and the Gschnitzstadial in the Maritime Alps according to ^{10}Be cosmogenic dating. *Boreas* **37**: 245–253.

Federici PR, Ribolini A, Spagnolo M. 2017. Glacial history of the Maritime Alps from the last glacial maximum to the little ice age. *Geological Society, London, Special Publications* ***433*****(1)**: 137-159.

Fernández-Fernández JM, Palacios D, García-Ruiz JM, Andrés N, Schimmelpfennig I et al. 2017. Chronological and geomorphological investigation of fossil debris-covered glaciers in relation to deglaciation processes: A case study in the Sierra de La Demanda northern Spain. *Quaternary Science Reviews* **170**: 232-249.

Florineth D, Schlüchter C. 2000. Alpine evidence for atmospheric circulation patterns in Europe during the Last Glacial Maximum. Quaternary Research, 54(3), 295-308.

Giardino JR, Shroder JF, Vitek JD, 1987. Rock glaciers. London: Allen & Unwin. 355 p.

Giguet-Covex C, Arnaud F, Poulenard J, Disnar JR, Delhon C, Francus P, David F, Enters D, Rey PJ, Delannoy JJ, 2011. Changes in erosion patterns during the Holocene in a *currently* treeless subalpine catchment inferred from lake sediment geochemistry (Lake Anterne 2063 m a.s.l, NW French Alps): The role of climate and human activities. *The Holocene* **21:** 651–665.

Gosse JC, Phillips FM. 2001. Terrestrial in situ cosmogenic nuclides: theory and application. *Quaternary Science Reviews* **20**: 1475-1560.

Hippolyte JC, Brocard G, Tardy M, et al. 2006. The recent fault scarps of the Western Alps (France): Tectonic surface rupture or gravitational sackung scarps? A combined mapping, geomorphic levelling and 10Be dating approach. *Tectonophysics* **418**: 255-276.

Hippolyte JC, Bourlès D, Braucher R, Carcaillet J, Léanni L, Arnold M, Aumaitre G, 2009. Cosmogenic^{10}Be dating of a sackung and its faulted debris covered glaciers in the Alps of Savoy France. *Geomorphology* **108**: 312-320.

Hormes A, Müller BU, Schlüchter C. 2001. The Alps with little ice: Evidence of eight Holocene phases of reduced glacier extent in the central Swiss Alps. *The Holocene* **11**: 255-265.

Hormes A, Beer J, Schlüchter C. 2006. A geochronological approach to understanding the role of solar activity on Holocene glacier length variability in the Swiss Alps. *Geografiska Annaler ser, A Physical Geography* **88**: 281-294.

Hughes PD, Woodward, JC, Gibbard PL. 2006. Late Pleistocene glaciers and climate in the Mediterranean. *Global and Planetary Change* **50**: 83-98.

Hughes PD, Fink D, Rodés Á, Fenton CR, Fujioka T. 2018. Timing of Pleistocene glaciations in the High Atlas, Morocco: New ^{10}Be and ^{36}Cl exposure ages. *Quaternary Science Reviews* **180**: 193-213.

Ivy-Ochs S, Kerschner H, Reuther A, Preusser F, Sailer R, Schaefer J, Kubik PW, Synal H, A, Schlüchter C. 2006a. The timing of glacier advances in northern European Alps based on surfaces exposure dating with cosmogenic^{10}Be ^{26}Al ^{36}Cl and ^{21}Ne in Siame LL et al., (eds.) In situ-produced cosmogenic nuclides and quantification of geological processes. *Geological Society of America Special Paper* **415**: 43-60,

Ivy-Ochs S, Kerschner H, Kubik PW., Schlüchter C. 2006b. Glacier response in the European Alps to Heinrich Event 1 cooling: the Gschnitz stadial. *Journal of Quaternary science* **21(2)**: 115-130.

Ivy-Ochs S, Kerschner H, Reuther A, Preusser F, Heine K, Maisch M, Kubik PW, Schlüchter C. 2008. Chronology of the last glacial cycle in the European Alps. *Journal of Quaternary Science* **23(6-7)**: 559-573.

Ivy-Ochs S, Kerschner H, Maisch M, Christl M, W, Kubik P, Schlüchter C. 2009. Latest Pleistocene and Holocene glacier variations in the European Alps. *Quaternary Science Reviews* **28**: 2137-2149.

Joerin UE, Stocker TF, Schlüchter C. 2006. Multicentury glacier fluctuations in the Swiss Alps during the Holocene. *The Holocene* **16**: 697-704,

Joerin UE, Nicolussi K, Fisher A, Stocker TF, Schlüchter C. 2008. Holocene optimum events inferred from subglacial sediments at Tschierva glacier eastern Swiss Alps. *Quaternary Science Reviews* **27**: 337-350.

Jorda M, Rosique T. 1994. Le tardiglaciaire des Alpes françaises du Sud: Rythme et modalités deschangements biomorphoclimatiques. *Quaternaire* **5**: 141-149.

Jorda M, Rosique T, Evin J. 2000. Données nouvelles sur l'âge du dernier maximum glaciaire dans les Alpes meridionales françaises. *C. R. Acad. Sci. Ser. IIA Earth Planet. Sci.* **331**: 187-193.

Julian M. 1980. Les Alpes maritimes Franco-Italiennes Etude géomorphologique. Atelier de reproduction des thèses, Université de Lille III, Lille, 836pp.

Kelly MA, Buoncristiani JF, Schlüchter C. 2004. A reconstruction of the last glacial maximum (LGM) ice-surface geometry in the western Swiss Alps and contiguous Alpine regions in Italy and France. *Eclogae Geologicae Helvetiae* **97(1)**: 57-75,

Kelly M, Ivy-Ochs S, Kubik P, Von Blackenburg F. 2006. Chronology of deglaciation based on ^{10}Be dates of glacial erosional features in the Grimsel Pass region central Swiss Alps. *Boreas* **35**: 634-643,

Kerschner H, Hertl A, Gross G, Ivy-Ochs S, Kubik PW. 2006. Surface exposure dating of moraines in the Kromer valley Silvretta Mountains Austria) – evidence for glacial response to the 8.2 ka event in the Eastern Alps. *The Holocene* **16**: 7-15.

Korschinek G, Bergmaier A, Faestermann T, Gerstmann UC, et al., 2010. A new value for the half-life of ^{10}Be by Heavy-Ion Elastic Recoil Detection and liquid scintillation counting. *Nuclear Instruments and Methods in Physics Research* **B**: 187-191.

Leemann A, Niessen F. 1994. Holocene glacial activity and climatic variations in the Swiss Alps: Reconstructing a continuous record from proglacial lake sediments. *The Holocene* **4**: 259-268.

Maisch M. 1992. Die Gletscher Graubündens, Rekonstruktion und Auswertung der Gletscher und deren Veränderungenseit dem Hochstand von 1850 im Gebiet der östlichen Schweizer Alpen Bündnerland und angrenzende Regionen. *Physische Geographie* **331**: 33B.

Merchel YS, Herpers U. 1999. An update on radiochemical separation techniques for the determination of long-lived radionuclides via accelerator mass spectrometry. *Radiochimica acta* **84**: 215-219.

Merchel, S., Arnold, M., Aumaître, G., Benedetti, L., Bourlès, D. L., Braucher, R., Alfimov, V., Freeman, S.P.H.T., Steier, P., Wallner, A., 2008. Toward more precise ^{10}Be and ^{36}Cl data from measurements at the 10^{-14} level: Influence of sample preparation. *Nuclear Instruments and Methods in Physics Research Section B: Beam Interactions with Materials and Atoms* 266.

Mix A, C, Bard E, Schneider R. 2001. Environmental processes of the ice age: land oceans glaciers EPILOG. *Quaternary Science Reviews* **20**: 627-657.

Monnier S, Kinnard C. 2015. Reconsidering the glacier to debris covered glacier transformation problem: New insights from the central Andes of Chile. *Geomorphology* **238**: 47-55,

Mourier B, Poulenard J, Carcaillet C, Williamson D. 2010. Soil evolution and subalpine ecosystem changes in the French Alps inferred from geochemical analysis of lacustrine sediments. *Journal of Paleolimnology*, doi: 10.1007/s10933-010-9438-0

Nicolussi K, Kaufmann M, Patzelt G, Van der Plicht J, Thurner A. 2005. Holocene tree-line variability in the Kauner Valley central eastern Alps indicated by dendrochronological analysis of living trees and subfossil logs. *Vegetation Hist. Archaeobot.* **14**: 221-234.

Nishiizumi K, Imamura M, Caffee MW, Southon JR, Finkel R, C, McAninch J. 2007. Absolute calibration of ^{10}Be AMS standards. *Nuclear Instruments and methods in Physics Research Section B: Beam Interactions with Materials and Atoms* **258**: 403-413.

Palacios D, García-Ruiz J, M, Andrés N, Schimmelpfennig I, Campos N, Léanni L. ASTER Team, 2017. Deglaciation in the central Pyrenees during the Pleistocene–Holocene transition: Timing and geomorphological significance. *Quaternary Science Reviews* **162**: 111-127.

Petersen J, Wilhelm B, Revel M, Rolland Y, Crouzet C, Arnaud F, Brisset E, Chaumillon E, Magand O. 2014. Sediments of Lake Vens (SW European Alps France) record large-magnitude earthquake events. *J. Paleolimnol.* **51:** 343-355.

Petit C, Goren L, Rolland Y, Bourlès D, Braucher R, Saillard M, Cassol D. 2017. Recent climate-driven river incision rate fluctuations in the Mercantour crystalline massif southern French Alps. *Quaternary Science Reviews* **165**: 73-87.

Rau F, Mauz F, Vogt S, Khalsa SJS, Raup B. 2005. Illustrated GLIMS Glacier Classification Manual Institut für Physische Geographie Freiburg Germany 36 pp.

Ribolini A, Chelli A, Guglielmin M, Pappalardo M. 2007. Relationships between glacier and debris covered glacier in the Maritime Alps Schiantala Valley Italy. *Quaternary Research*, doi:10.1016/j.yqres.2007.08.004.

Rolland Y, Petit C, Saillard M, Braucher R, Bourlès D, Darnault R, Cassol D, ASTER Team. 2017. Inner gorges incision history: a proxy for deglaciation? Insights from Cosmic Ray Exposure dating ^{10}Be and ^{36}Cl of river-polished surfaces Tinée River SW Alps France. *Earth and Planetary Science Letters* **457**: 271-281.

Saillard M, Petit C, Rolland Y, Braucher R, Bourlès DL, Zerathe S, Revel M, Jourdon A. 2014. Late Quaternary incision rates in the Vésubie catchment area Southern French Alps) from in situ-produced ^{36}Cl cosmogenic nuclide dating: Tectonic and climatic implications. *Journal of Geophysical Research: Earth Surface* **119**: 2013JF002985.

Sanchez G, Rolland Y, Corsini M, Braucher R, Bourlès D, Arnold M, Aumaître G. 2010a. Relationships between tectonics slope instability and climate Change: Cosmic ray exposure dating of active faults landslides and glacial surfaces in the SW Alps. *Geomorphology* **117**: 1-13.

Sanchez G, Rolland Y, Schreiber D, Corsini M, Lardeaux J.M, Giannerini G, 2010b. The active fault system of SW Alps. *Journal of Geodynamics* **49**: 296-302.

Sanchez G, Rolland Y, Corsini M, Jolivet M, Brichaud S, Carter A. 2011. Exhumation controlled by transcurrent tectonics: the Argentera-Mercantour massif SW Alps. *Terra Nova* **23**: 116–126.

Schimmelpfennig I, Schaefer JM, Akçar N, Ivy-Ochs S, Finkel RC, Schlüchter C. 2012. Holocene glacier culminations in the Western Alps and their hemispheric relevance. *Geology* **40(10):** 891-894.

Schindelwig I, Akçar N, Kubik PW, et al. 2012. Lateglacial and early Holocene dynamics of adjacent valley glaciers in the Western Swiss Alps. *Journal of Quaternary Science* **27**: 114–124.

Siame LL, Braucher R, Bourlès DL. 2000. Les nucléidescosmogéniques produits in-situ ; de nouveaux outils en géomorphologie quantitative. *Bulletin de la Société Géologique de France* **171(4)**: 383-396.

Sircombe KN. 2004. Age display: an excel workbook to evaluate and display univariate geochronological data using binned frequency histograms and probability density distributions. *Computers & Geosciences* **30**: 21-31.

Soldati M, Corsini A, Pasuto A. 2004. Landslides and climate change in the Italian Dolomites since the Lateglacial. *Catena* **55**: 141-161.

Solomina ON, Bradley RS, Hodgson DA, et al. 2015. Holocene glacier fluctuations. *Quaternary Science Reviews* **111**: 9–34.

Stone JO. 2000. Air pressure and cosmogenic isotope production. *Journal of Geophysical Research* **105**, 753-760.

Tremblay MM, Shuster DL, Spagnolo M, Renssen H, Ribolini A. 2018. Temperatures recorded by cosmogenic noble gases since the last glacial maximum in the Maritime Alps. *Quaternary Research*. DOI: 10.1017/qua.2018.109

Wirsig C, Zasadni J, Ivy-Ochs S, Christl M, Kober F, Schlüchter C. 2016. A deglaciation model of the Oberhasli Switzerland, *Journal of Quaternary Science* **31(1)**: 46-59.

Zerathe S, Lebourg T, Braucher R, Bourlès D. 2014. Mid-Holocene cluster of large-scale landslides revealed in the Southwestern Alps by ^{36}Cl dating, Insight on an Alpine-scale landslide activity. *Quaternary Science Reviews* **90**: 106-127.

Figures

Figure 1. A, Localization of study area, the Upper Tinée River in SW Alps (France). 1 position of Eastern Ecrins Massif's glacier du Sélé (Figs. 8A-B); 2 position of Miage glacier (Mont Blanc Massif). B, satellite image of SW Alps with the main rivers and location of Fig. 2. Red stripped line: Maximal advance of glaciers during the LGM, after Julian (1980), Darnault et al. (2012) and Brisset et al. (2015). On the Italian side, the Gesso catchment is the location of the Federici et al. studies (see Federici et al. 2008, 2011, 2017).

Figure 2. Shaded topography of the Tinée River catchment with glacial and fluvioglacial deposits (Faure-Muret, 1970) and ages of onset of fluvial incision following deglaciation (Rolland et al., 2017), after Petit et al. (2017). Dashed lines with white letters indicate the trimline of the Tinée glacier during the LGM (after Julian, 1980).

Figure 3. General geomorphological map of the South Mercantour Range slope.

Figure 4. Photographs of the Vens lakes study area, with the location of the collected samples, and representative pictures of the polished surfaces sampled for ^{10}Be CRE dating.

Figure 5. Google image of Vens area, showing the location of dated samples with the main geomorphological features related to glacier activity (see Fig. 6 for details and interpretation).

Figure 6. Detailed geomorphological map of the upper Vens Valley, modified from Darnault (2012) and Brisset et al. (2015). The red stars represent the locations of the samples dated using the ^{10}Be CRE dating method.

Figure 7. Polished glacial bedrock sample ^{10}Be CRE age distribution reported at a 1σ level by a binned frequency histogram and probability and density curves (Sircombe 2004). The density curve is fitted by a filter of concordance, with a fixed confidence level of 95%. The age ranges are determined according to the density curve distribution. Curve A: Distribution representation of all samples; Curve B: Distribution representation of the Fourchas Lake area samples; Curve C: Distribution representation of ages the Vens Lake area samples.

Figure 8. A, Photograph of the frontal part and lateral moraines of the 'Glacier Noir' in the Ecrins Massif (location 1 in Fig. 1A). B, Lateral moraine in the upper part of the Sélé Valley (also in the Ecrins Massif). The approximate thickness of the moraine in its upper part is 30 meters. Note the variable extent of erosion, exhuming zones of polished crystalline basement to the left of the photo, while the thickness of moraine remains is very large downstream.

Figure 9. Graphic illustrating the average soil thickness required to obtain ^{10}Be CRE ages of 15 ka, 11 ka or 8 ka. The blue column corresponds to the samples located in Fourchas Lake area, while the green column corresponds to the samples located in Vens Lake area.

Figure 10. Multi-proxy age-depth model of core VEN10-II. The model age is defined on the basis of ^{14}C AMS ages of terrestrial material sampled from the continuous lacustrine sedimentation, and palynostratigraphical, after Brisset et al. (2015) and Petersen et al. (2014).

Figure 11. Recalculated CRE ^{10}Be ages of basement geomorphologies on the Southern Slope of Tenibre peak (Fer and Rabuons valleys). A, Location of the Upper Fer Valley and Rabuons Lake, North of St Etienne de Tinée. B, Repartition of ages on the geomorphologies of the

Upper Fer Valley, south of Tenibre. C, Photograph of the left side of Fer Valley, looking towards the south. D, Probability curve of recalculated CRE ^{10}Be ages. Ages were recalculated with the recent parameters according to procedures described in Suppl. Mat. 2, for details see Darnault et al. (2012).

Figure 12. Synthesis of deglaciation ages obtained on both slopes of the Argentera Massif (this paper and Federici et al., 2017), and attempt to integrate them into a timetable for deglaciation history since the LGM.

Figure 13. Sketch of deglaciation phases in the Vens Valley since 15 ka. A, Early deglaciation after the LGM at 20-18 ka. B, State of the valley at the end of Vens-I (≥14.7 ka). Moraine boulders and sediment were deposited due to the glacier advance during the Vens I stadial. C, Situation of the valley before the end of the Vens-II glacial phase (9-8 ka). This latter glacier recession phase starts at the end of the Younger Dryas cold period (12 ka, Darnault et al. 2012). However, a certain amount of ice is maintained in the upper and least exposed part of the valley, in the form of a debris covered glacier. The ^{10}Be concentrations in samples from the upper part of the Vens Valley, and the nature of sediments in the Vens Lake core (Fig. 10) suggest that some ice was maintained from the end of Younger Dryas to about 8-9 ka, at 2400 m a.s.l. D, after 8-9 ka, the morphological features are ice-free, and the fine-grained moraine material was washed away, as shown by a change towards low sedimentation rates in the Vens sediment core. This time for moraine denudation and stabilization is also ascribed by the younger and variable ^{10}Be CRE ages from flat basement polished surfaces. Screes and moraines are fixed by vegetation because of soil development, as shown by palynological study of Brisset et al. (2015).

Tables

Table1.^{10}Be sample characteristics and exposure ages from the Vens Valley glacially polished surfaces.

Table 2. Table illustrating the height of soil column needed for each sample to reach ages of 15 ka, 11 ka and 8 ka exposure duration.

Suppl. Table 1. Recalculated CRE ages for the South Tenibre slope of Mercantour (Darnault et al., 2012).

Suppl. Mat. 1. Geological map of the Vens Valley (source: from infoterre.brgm.fr, modified).

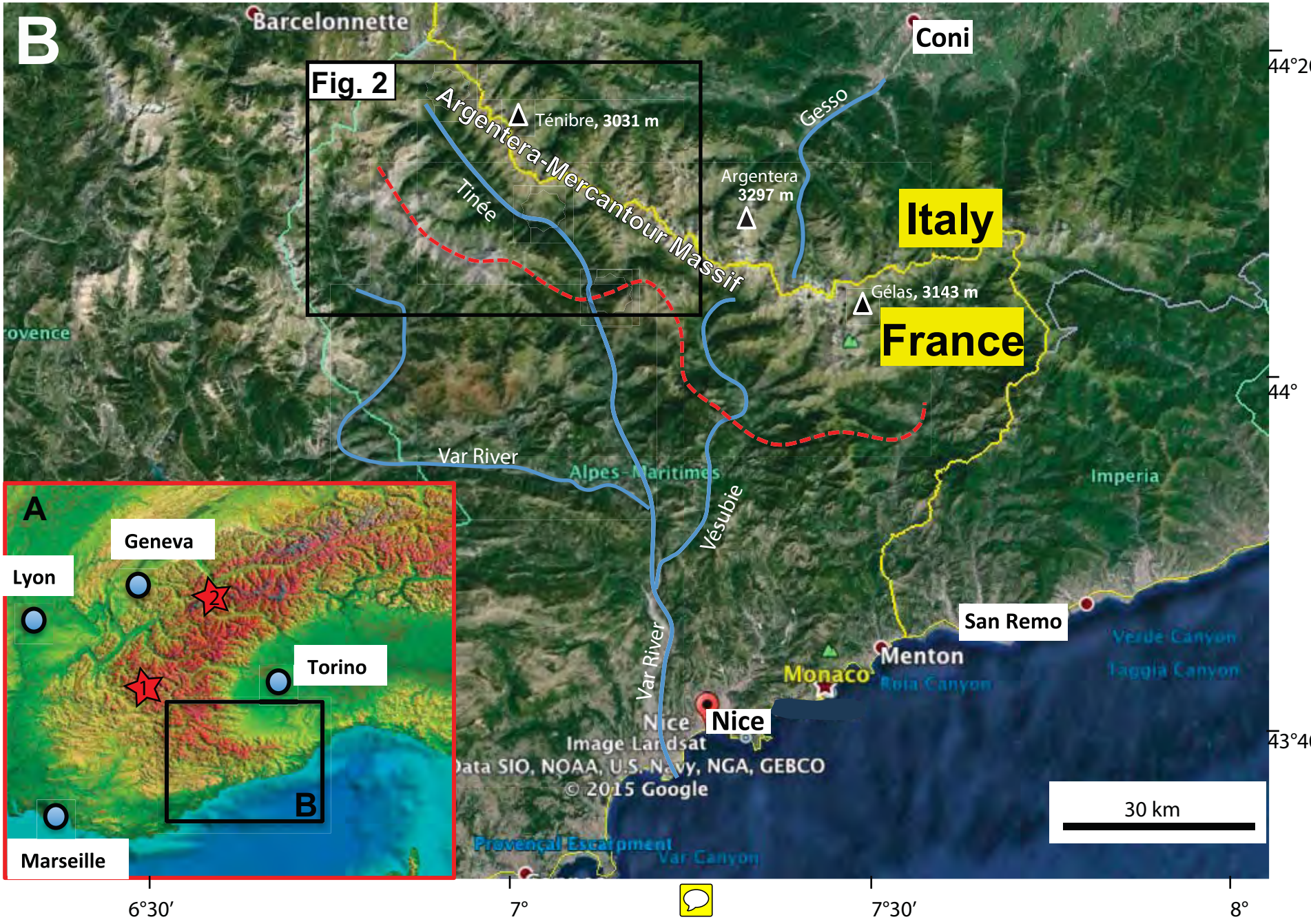
B
Barcelonnette
Coni
Fig. 2
Argentera-Mercantour Massif
Ténibre, 3031 m
Tinée
Gesso
Argentera
3297 m
Italy
Gélas, 3143 m
France
Var River
Alpes-Maritimes
Vésubie
Imperia
A
Geneva
Lyon
Torino
Marseille
1
2
B
San Remo
Menton
Monaco
Nice
Nice
Image Landsat
Data SIO, NOAA, U.S. Navy, NGA, GEBCO
© 2015 Google
Var River
Verde Canyon
Taggia Canyon
Roia Canyon
Provençal Escarpment
Var Canyon
30 km
44°20′
44°
43°40′
6°30′
7°
7°30′
8°

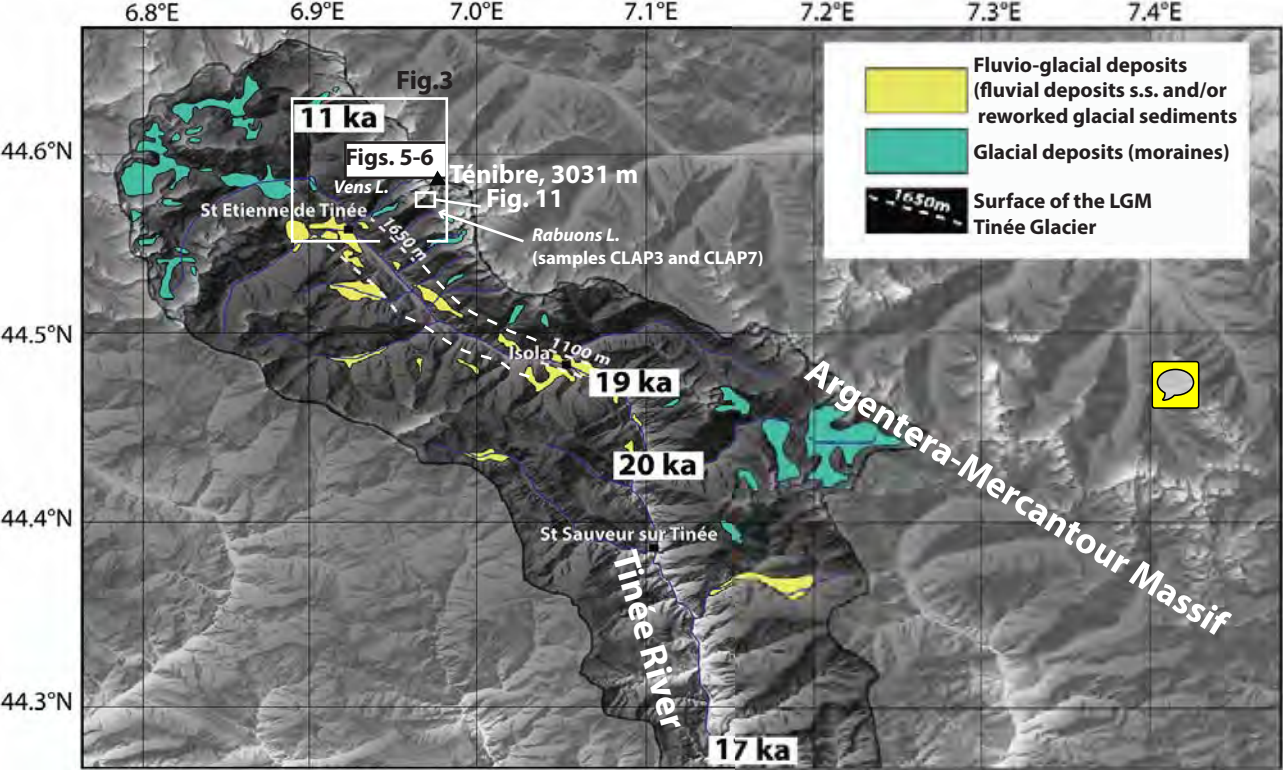
6.8°E
6.9°E
7.0°E
7.1°E
7.2°E
7.3°E
7.4°E
44.6°N
44.5°N
44.4°N
44.3°N
Fig.3
11 ka
Figs. 5-6
Ténibre, 3031 m
Fig. 11
Vens L.
St Etienne de Tinée
1650 m
Rabuons L.
(samples CLAP3 and CLAP7)
1100 m
Isola
19 ka
20 ka
St Sauveur sur Tinée
Tinée River
17 ka
Argentera-Mercantour Massif
Fluvio-glacial deposits
(fluvial deposits s.s. and/or
reworked glacial sediments
Glacial deposits (moraines)
1650m
Surface of the LGM
Tinée Glacier

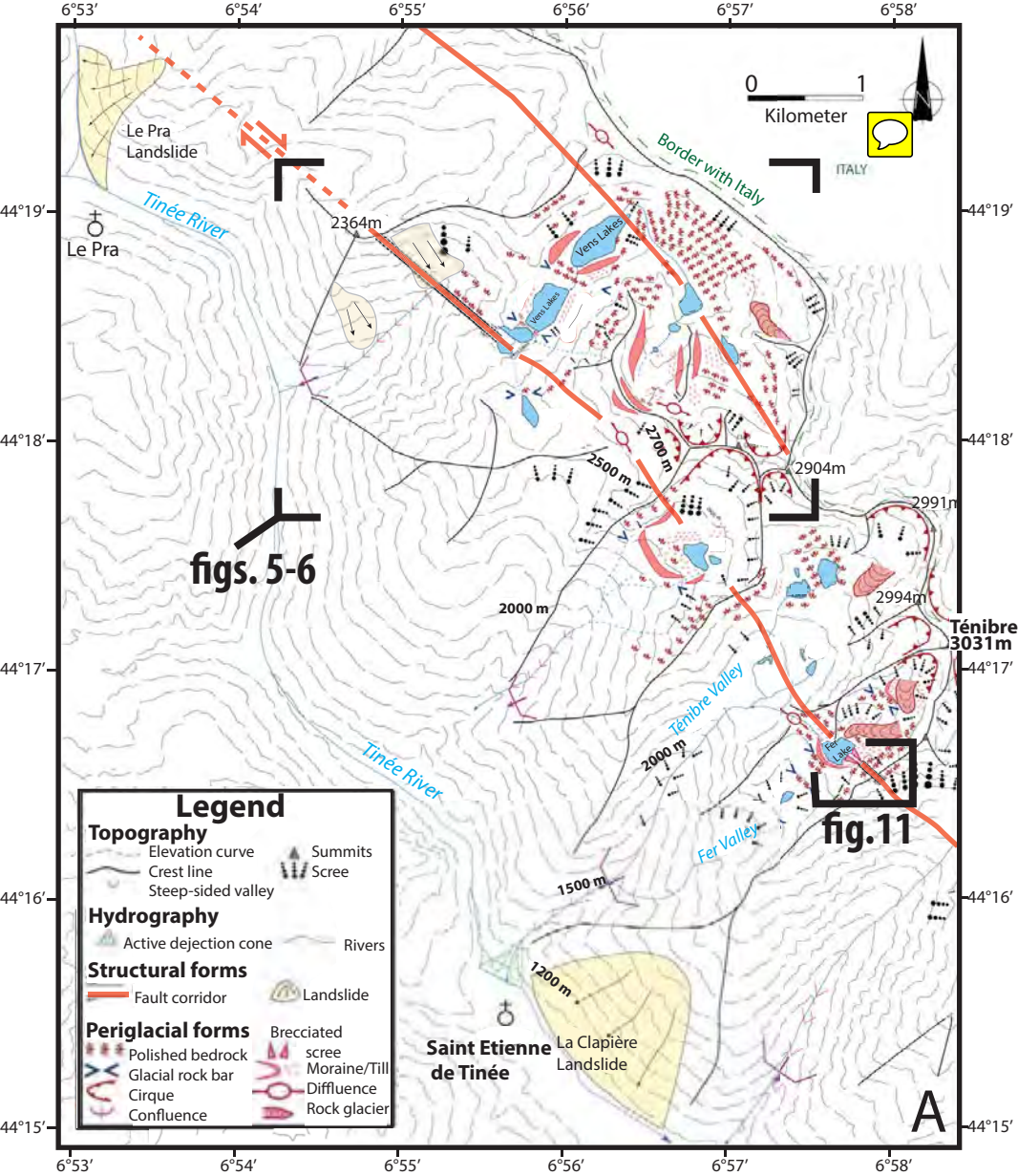
6°53′
6°54′
6°55′
6°56′
6°57′
6°58′
44°19′
44°18′
44°17′
44°16′
44°15′
0
1
Kilometer
N
Le Pra
Landslide
Tinée River
Le Pra
2364m
Border with Italy
ITALY
Vens Lakes
2700 m
2500 m
2904m
2991m
2994m
Ténibre
3031m
figs. 5-6
2000 m
Ténibre Valley
Fer Lake
fig.11
Fer Valley
1500 m
1200 m
Saint Etienne
de Tinée
La Clapière
Landslide
A
Legend
Topography
Elevation curve
Crest line
Steep-sided valley
Summits
Scree
Hydrography
Active dejection cone
Rivers
Structural forms
Fault corridor
Landslide
Periglacial forms
Polished bedrock
Glacial rock bar
Cirque
Confluence
Brecciated
scree
Moraine/Till
Diffluence
Rock glacier

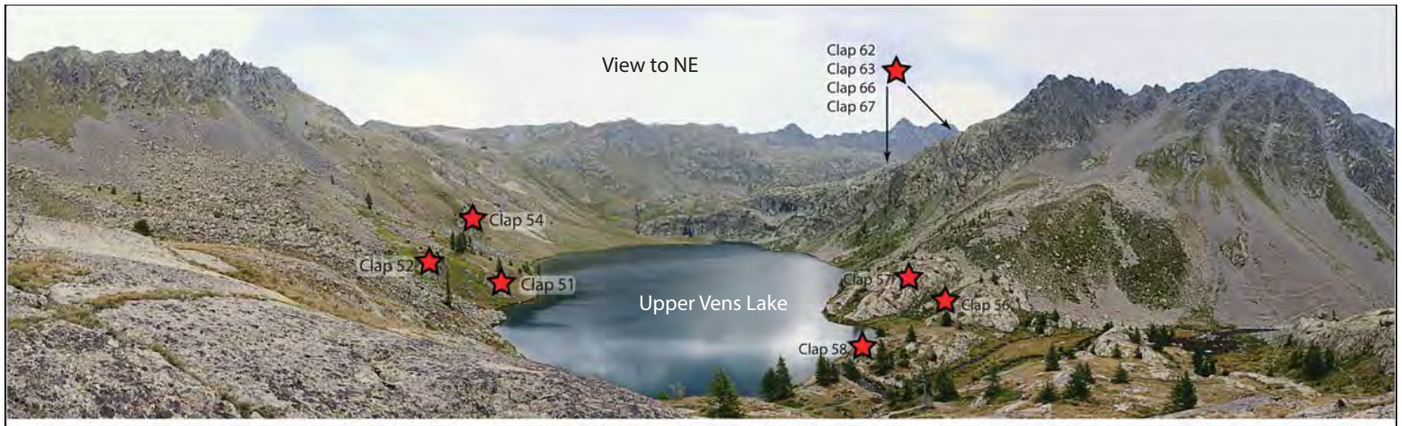
View to NE
Clap 62
Clap 63
Clap 66
Clap 67
Clap 54
Clap 52
Clap 51
Upper Vens Lake
Clap 57
Clap 56
Clap 58


Clap 66
Fourchas Lake


Clap 63


Clap 58

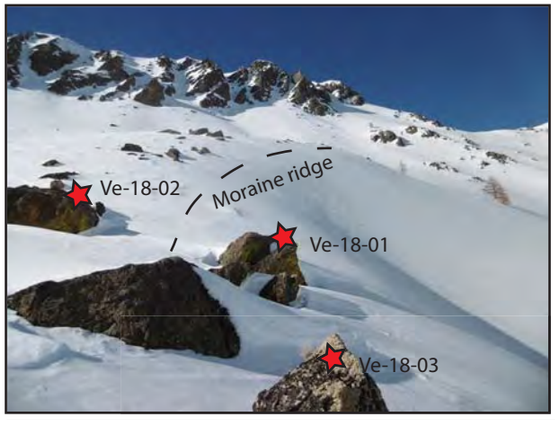
Ve-18-02
Moraine ridge
Ve-18-01
Ve-18-03

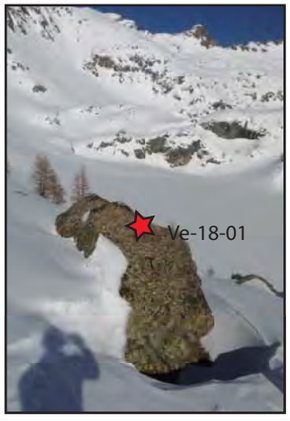
Ve-18-01


Clap 51


View to NW
Clap67
Clap62
Fourchas Lake


Clap67
Glacial Striae

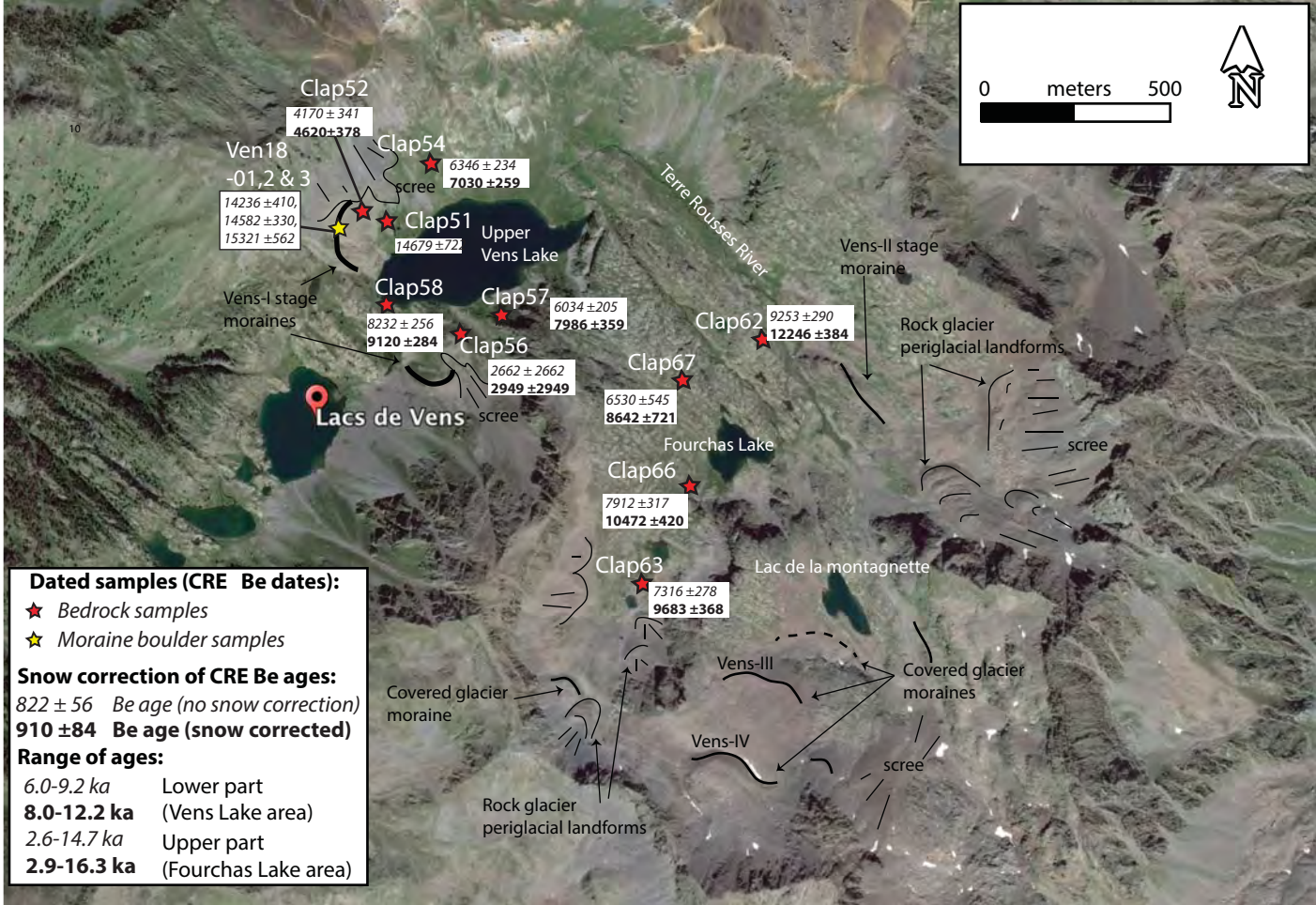
0 meters 500
N
Clap52
4170 ± 341
4620±378
Ven18
-01,2 & 3
14236 ±410,
14582 ±330,
15321 ±562
Clap54
6346 ± 234
7030 ±259
scree
Clap51
14679 ±721
Upper
Vens Lake
Terre Rousses River
Vens-I stage
moraines
Clap58
8232 ± 256
9120 ±284
Clap57
6034 ±205
7986 ±359
Clap56
2662 ± 2662
2949 ±2949
scree
Lacs de Vens
Clap62
9253 ±290
12246 ±384
Vens-II stage
moraine
Rock glacier
periglacial landforms
Clap67
6530 ±545
8642 ±721
Fourchas Lake
scree
Clap66
7912 ±317
10472 ±420
Clap63
7316 ±278
9683 ±368
Lac de la montagnette
Vens-III
Covered glacier
moraines
Covered glacier
moraine
Vens-IV
scree
Rock glacier
periglacial landforms
Dated samples (CRE Be dates):
Bedrock samples
Moraine boulder samples
Snow correction of CRE Be ages:
822 ± 56 Be age (no snow correction)
910 ±84 Be age (snow corrected)
Range of ages:
6.0-9.2 ka
8.0-12.2 ka
Lower part
(Vens Lake area)
2.6-14.7 ka
2.9-16.3 ka
Upper part
(Fourchas Lake area)

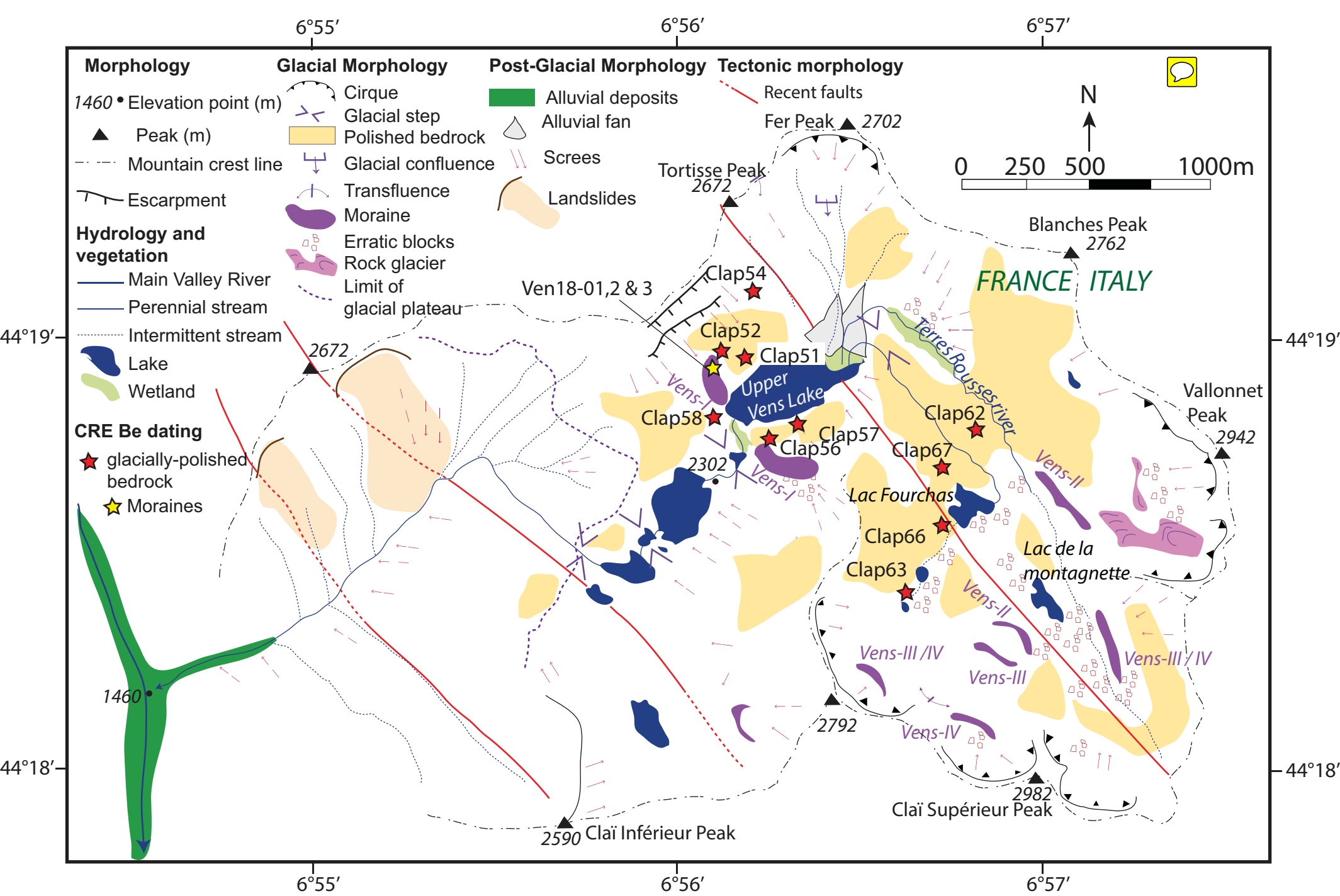
6°55′
6°56′
6°57′
44°19′
44°18′
Morphology
1460 Elevation point (m)
Peak (m)
Mountain crest line
Escarpment
Hydrology and vegetation
Main Valley River
Perennial stream
Intermittent stream
Lake
Wetland
CRE Be dating
glacially-polished bedrock
Moraines
Glacial Morphology
Cirque
Glacial step
Polished bedrock
Glacial confluence
Transfluence
Moraine
Erratic blocks
Rock glacier
Limit of glacial plateau
Post-Glacial Morphology
Alluvial deposits
Alluvial fan
Screes
Landslides
Tectonic morphology
Recent faults
N
0 250 500 1000m
Fer Peak 2702
Tortisse Peak 2672
Blanches Peak 2762
FRANCE ITALY
Ven18-01,2 & 3
Clap54
Clap52
Clap51
Clap58
Clap57
Clap56
Clap62
Clap67
Clap66
Clap63
Upper Vens Lake
Vens-I
Vens-II
Vens-III /IV
Vens-III
Vens-IV
Terres Rousses river
Lac Fourchas
Lac de la montagnette
Vallonnet Peak 2942
2672
2302
1460
2792
2982
Claï Supérieur Peak
2590
Claï Inférieur Peak

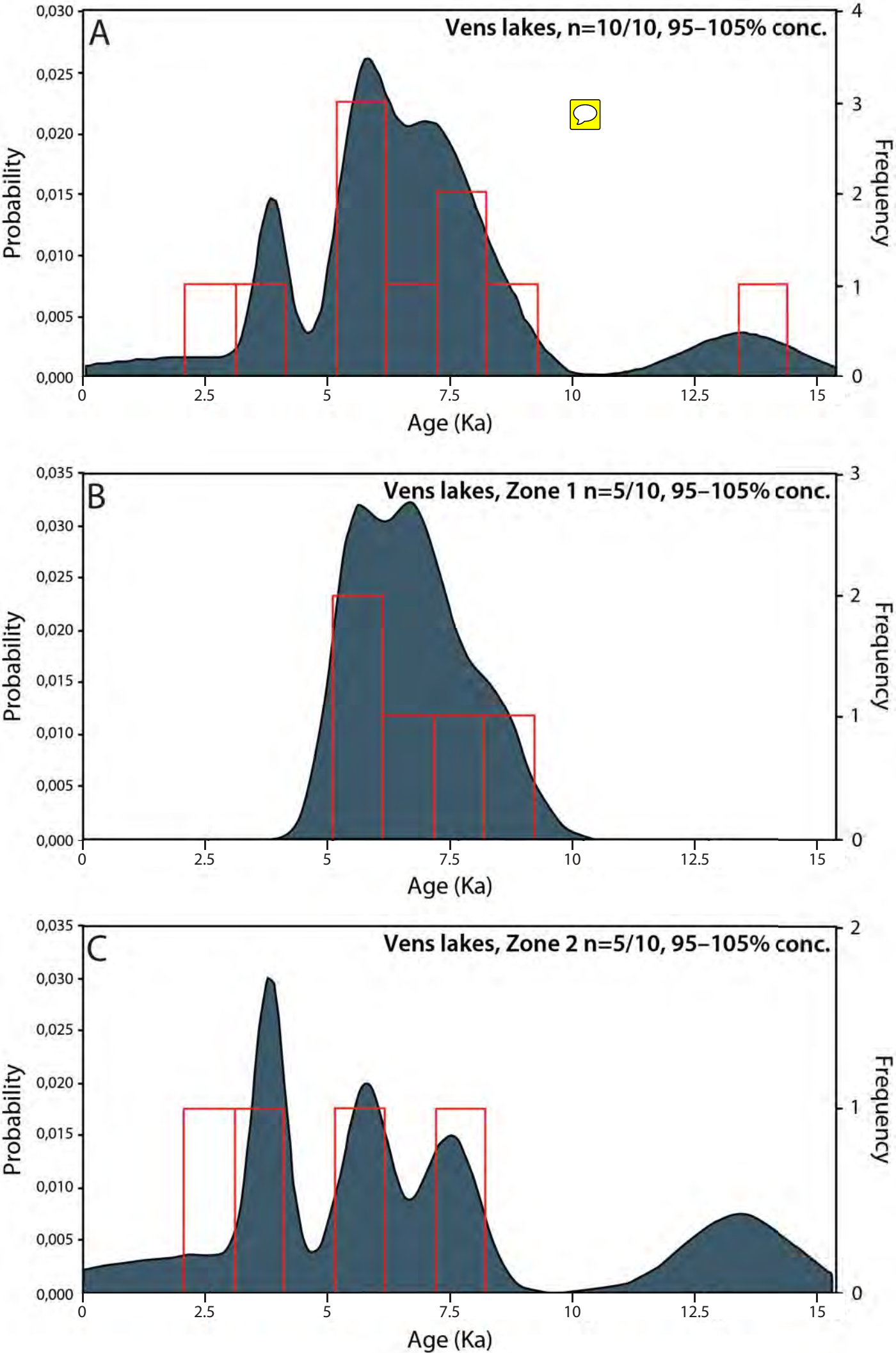
A
Vens lakes, n=10/10, 95–105% conc.
Probability
Frequency
Age (Ka)
B
Vens lakes, Zone 1 n=5/10, 95–105% conc.
Probability
Frequency
Age (Ka)
C
Vens lakes, Zone 2 n=5/10, 95–105% conc.
Probability
Frequency
Age (Ka)


A


B

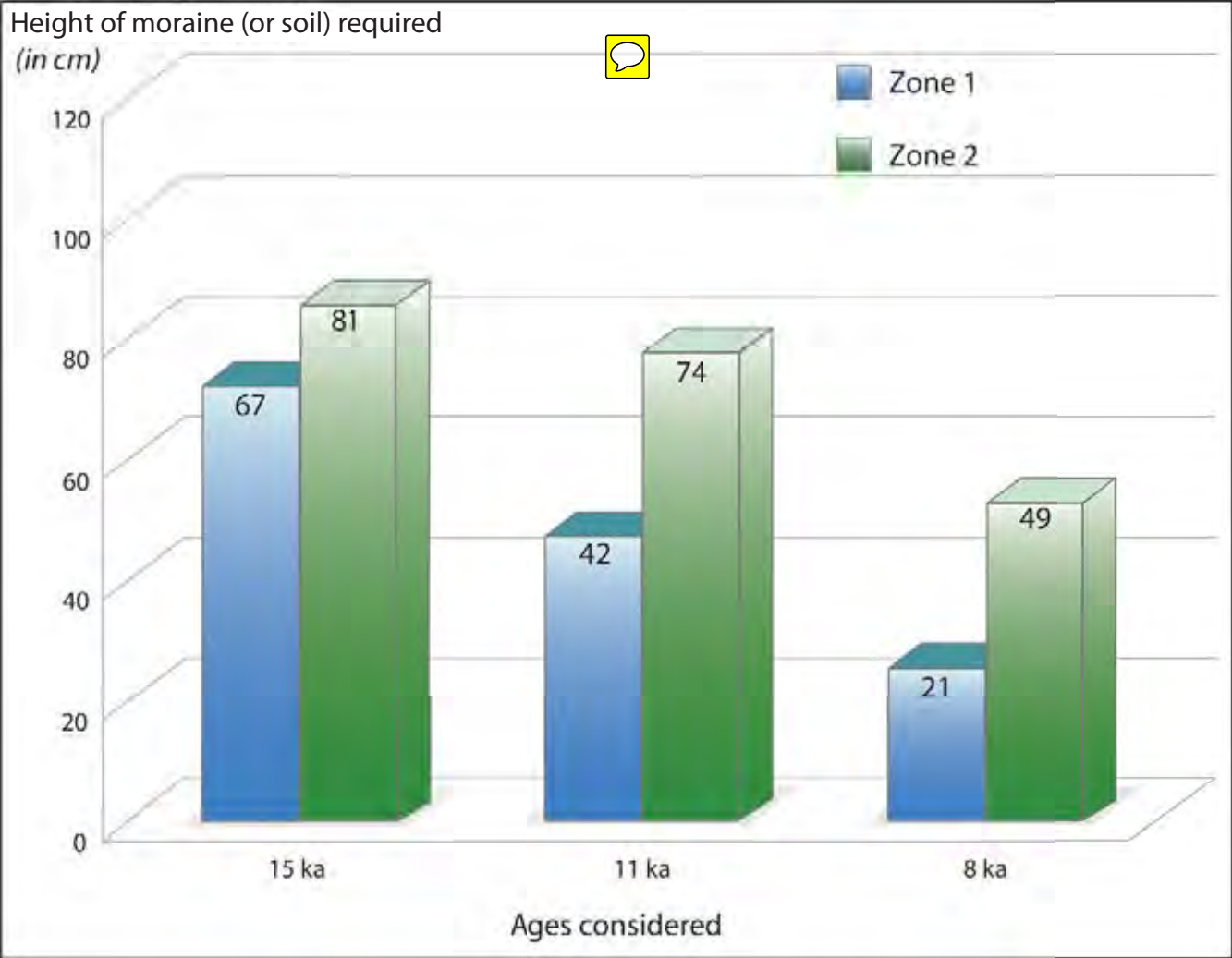
Height of moraine (or soil) required
(in cm)
120
100
80
60
40
20
0
Zone 1
Zone 2
67
81
42
74
21
49
15 ka
11 ka
8 ka
Ages considered

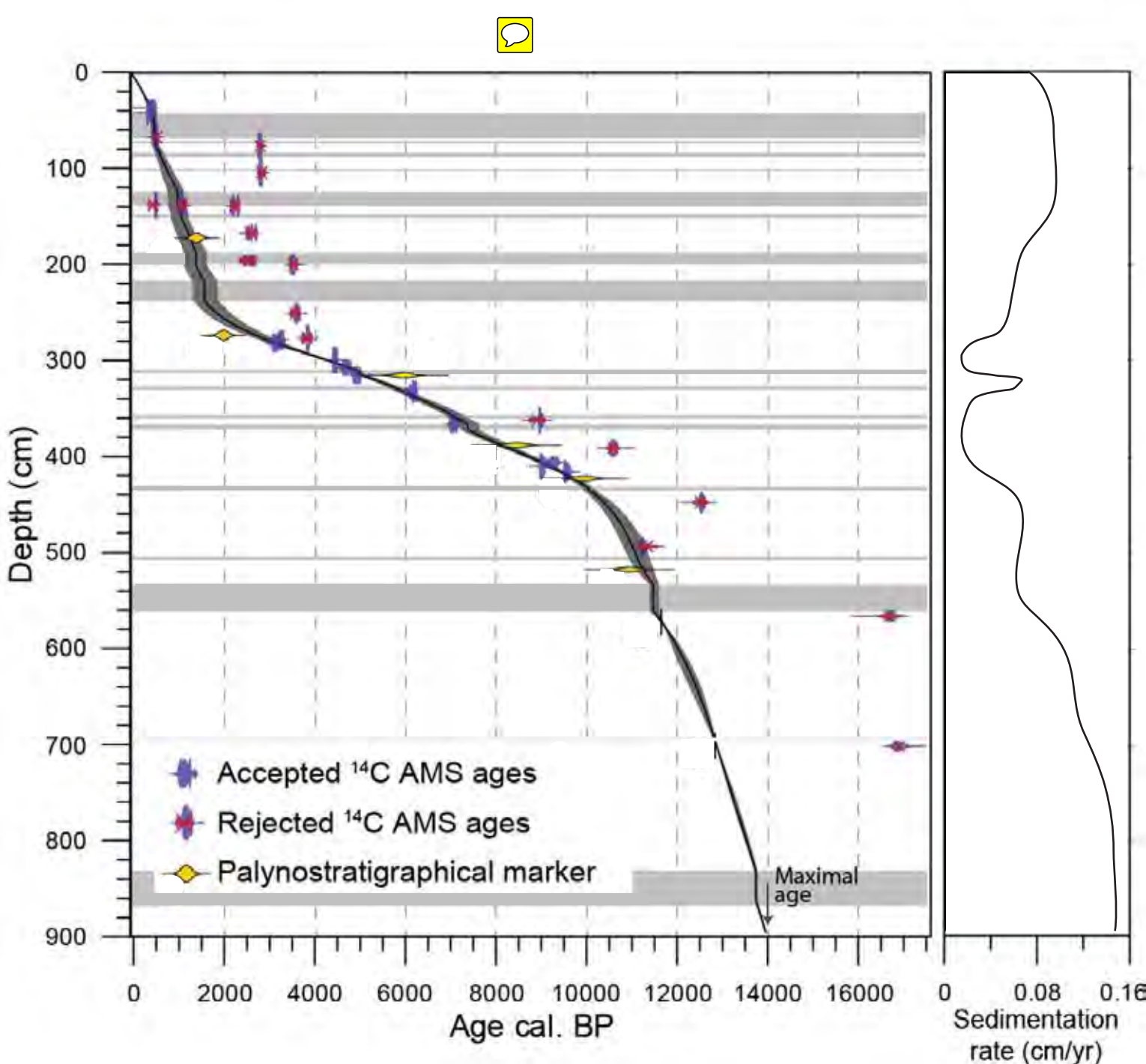
Depth (cm)
0
100
200
300
400
500
600
700
800
900
Accepted ¹⁴C AMS ages
Rejected ¹⁴C AMS ages
Palynostratigraphical marker
Maximal age
0
2000
4000
6000
8000
10000
12000
14000
16000
Age cal. BP
0
0.08
0.16
Sedimentation rate (cm/yr)

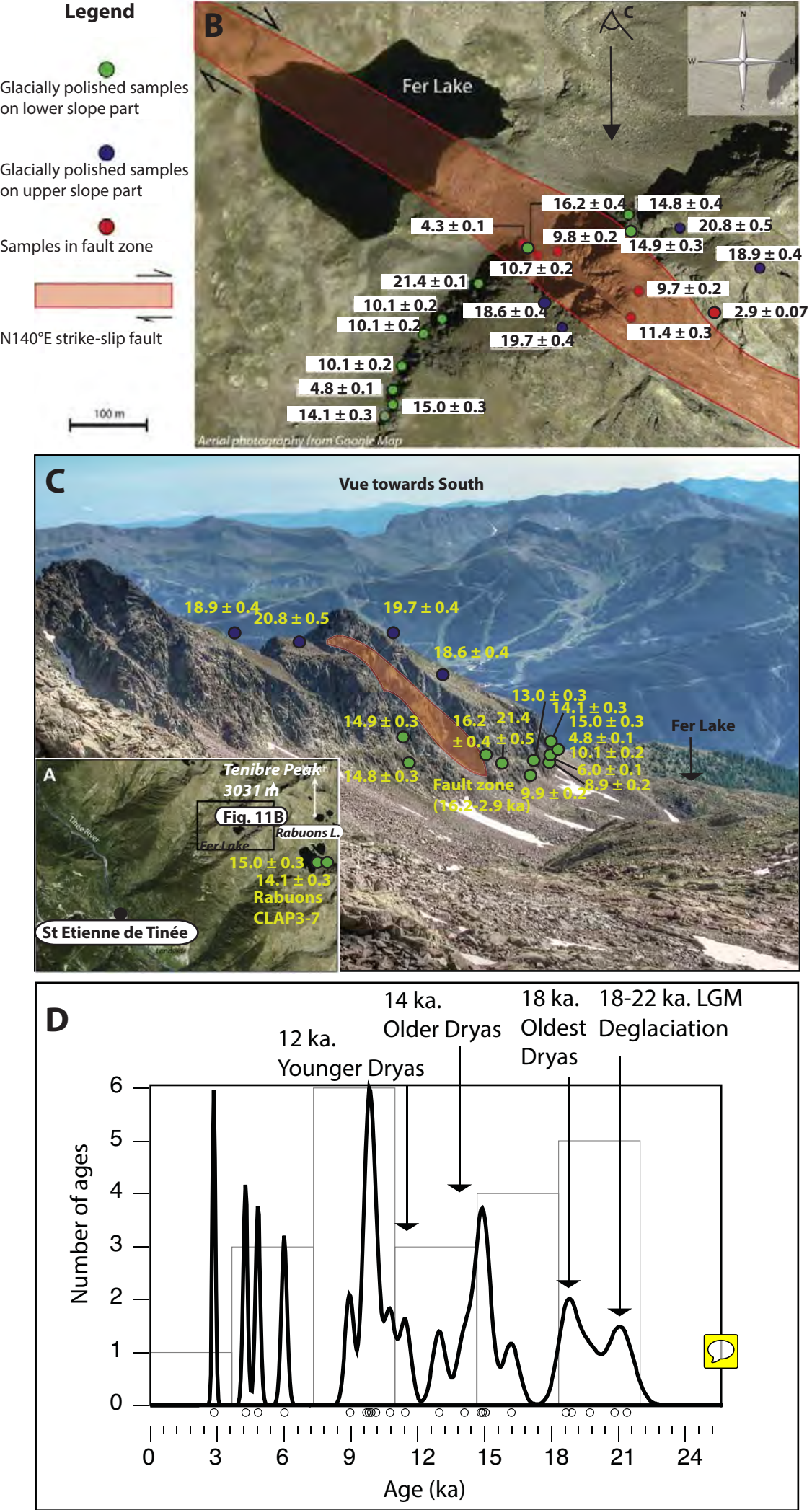
Legend
Glacially polished samples on lower slope part
Glacially polished samples on upper slope part
Samples in fault zone
N140°E strike-slip fault
100 m
B
Fer Lake
16.2 ± 0.4
14.8 ± 0.4
4.3 ± 0.1
20.8 ± 0.5
9.8 ± 0.2
14.9 ± 0.3
18.9 ± 0.4
10.7 ± 0.2
21.4 ± 0.1
9.7 ± 0.2
10.1 ± 0.2
18.6 ± 0.4
2.9 ± 0.07
10.1 ± 0.2
11.4 ± 0.3
19.7 ± 0.4
10.1 ± 0.2
4.8 ± 0.1
14.1 ± 0.3
15.0 ± 0.3
Aerial photography from Google Map
C
Vue towards South
18.9 ± 0.4
20.8 ± 0.5
19.7 ± 0.4
18.6 ± 0.4
13.0 ± 0.3
14.1 ± 0.3
14.9 ± 0.3
16.2 ± 0.4
21.4 ± 0.5
15.0 ± 0.3
4.8 ± 0.1
10.1 ± 0.2
6.0 ± 0.1
8.9 ± 0.2
14.8 ± 0.3
Fault zone (16.2-2.9 ka)
9.9 ± 0.2
Fer Lake
A
Tenibre Peak 3031 m
Fig. 11B
Rabuons L.
Fer Lake
15.0 ± 0.3
14.1 ± 0.3
Rabuons CLAP3-7
St Etienne de Tinée
D
12 ka. Younger Dryas
14 ka. Older Dryas
18 ka. Oldest Dryas
18-22 ka. LGM Deglaciation
Number of ages
0
1
2
3
4
5
6
0
3
6
9
12
15
18
21
24
Age (ka)

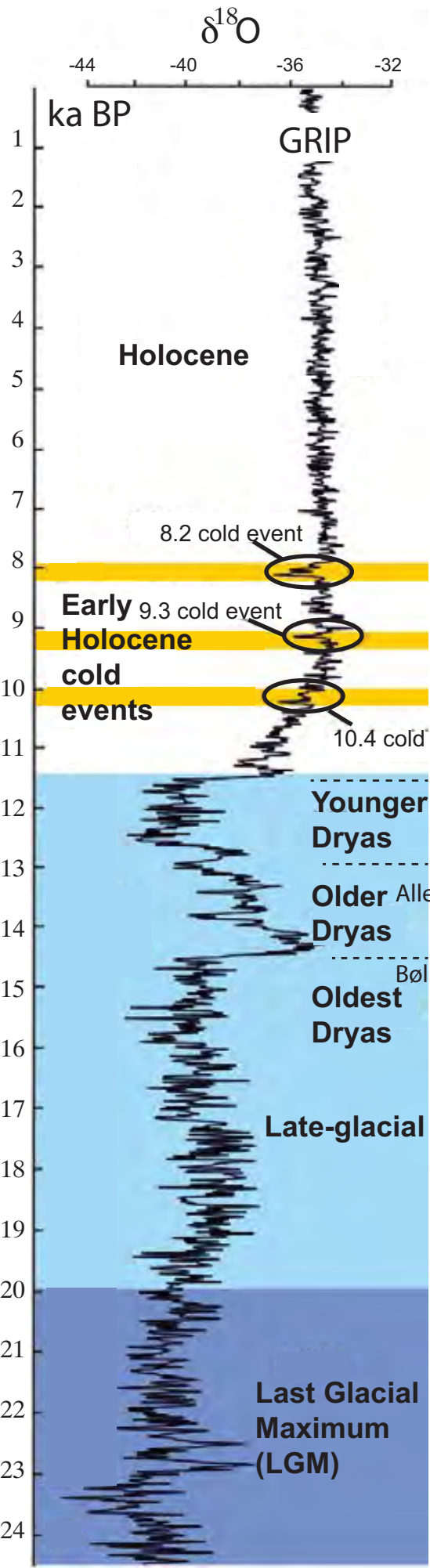

Vens-IV deglaciation = Little Ice Age?

End of moraine erosion/stabilization

End of «glacial milk» sediments in Vens Lake
Vens-III deglaciation?

Rock glacier in Upper vens valley

Vens-II deglaciation

glaciers reformed in high altitude areas (Vens-II)

Onset of Vens Lake sedimentation
Summit lower slopes are free of ice (S slope)

Vens-I deglaciation

Mercantour summit slopes free of ice (S slope)
Bühl stadial low valley moraines (N slope)

LGM deglaciation

LGM lower valley frontal moraine (N slope)

(A) Post LGM (20-18 ka)

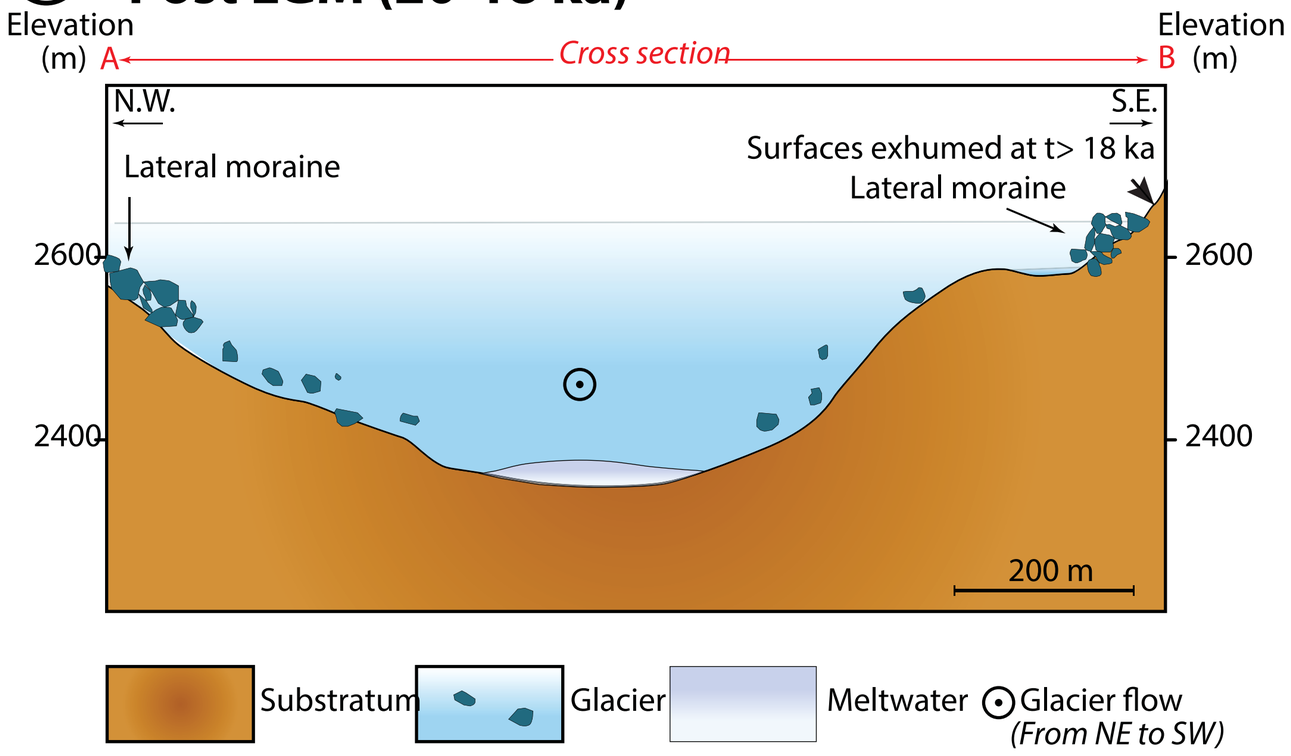

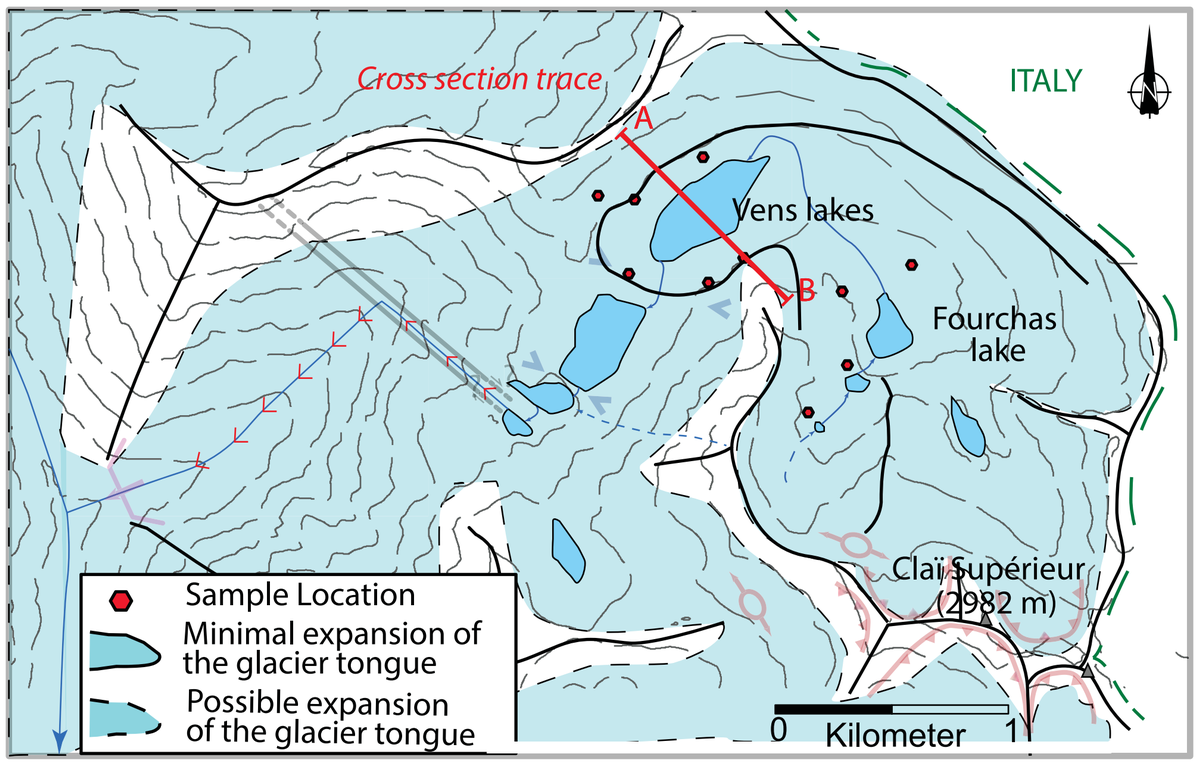

(B) Vens-I (>14-15 ka)

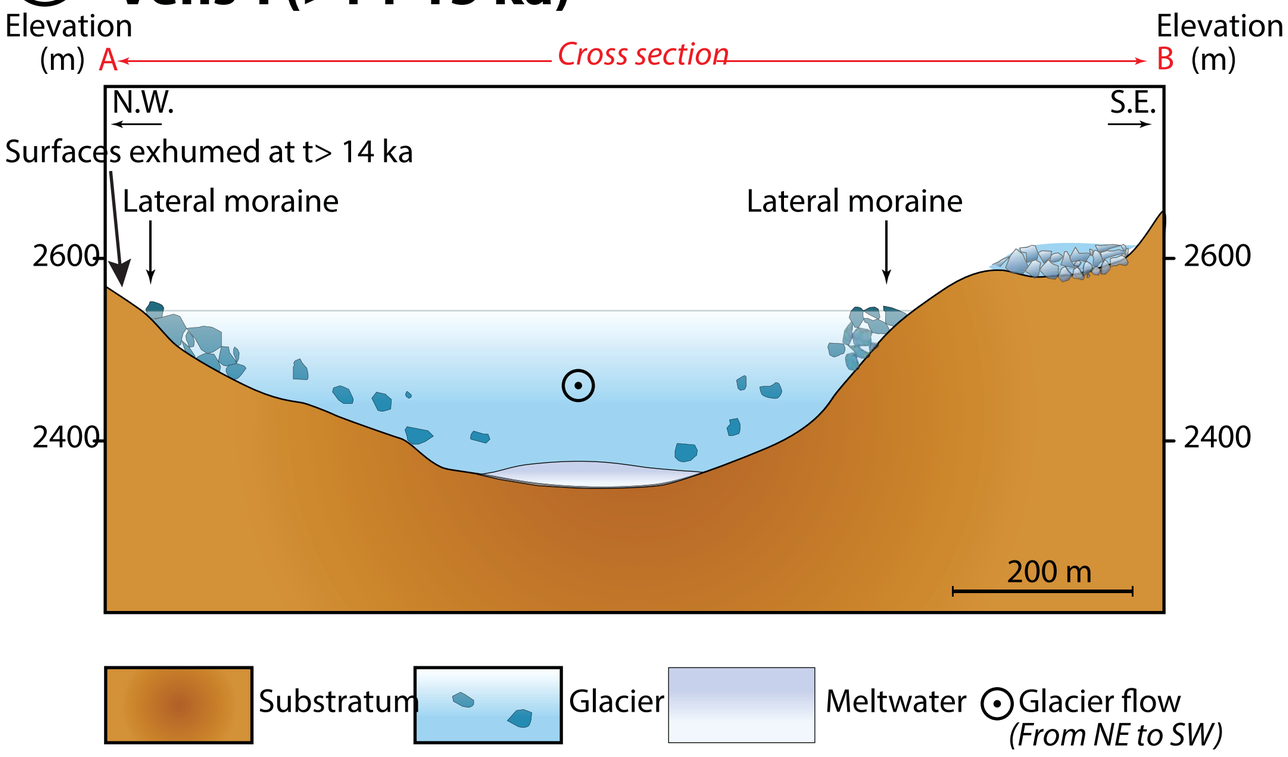

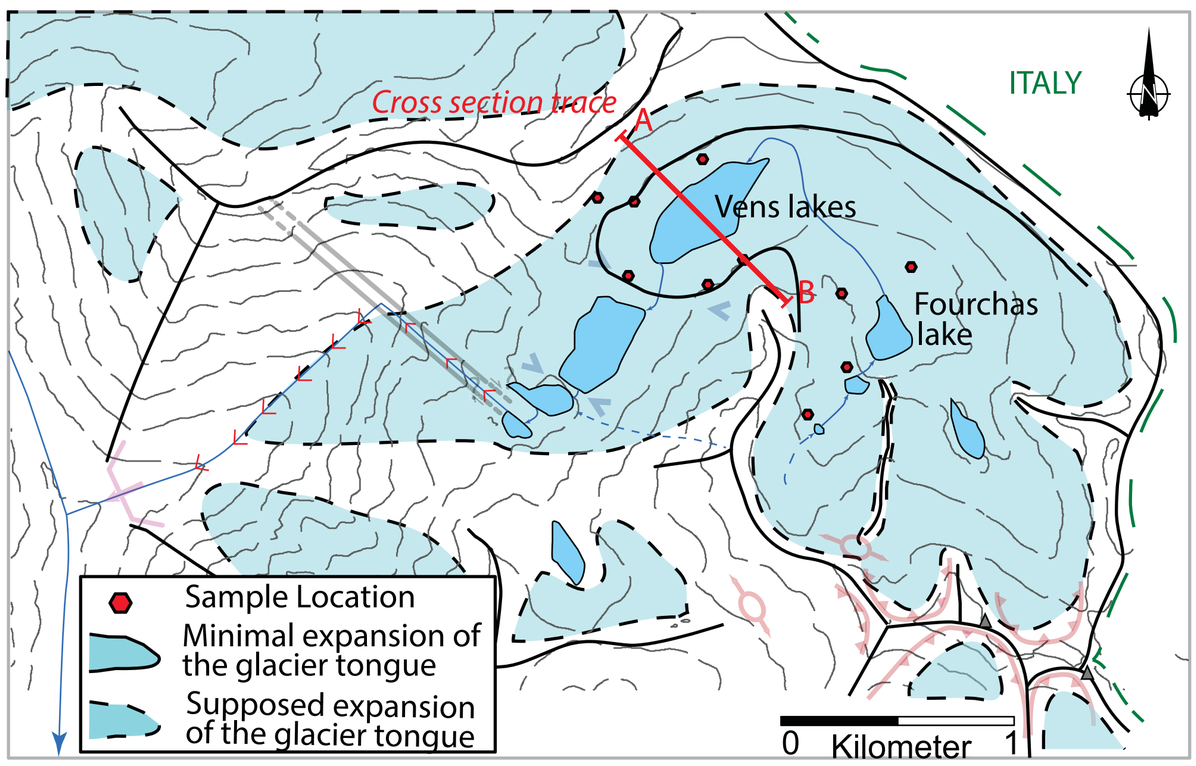

(C) Vens-II (12-9.8 ka)

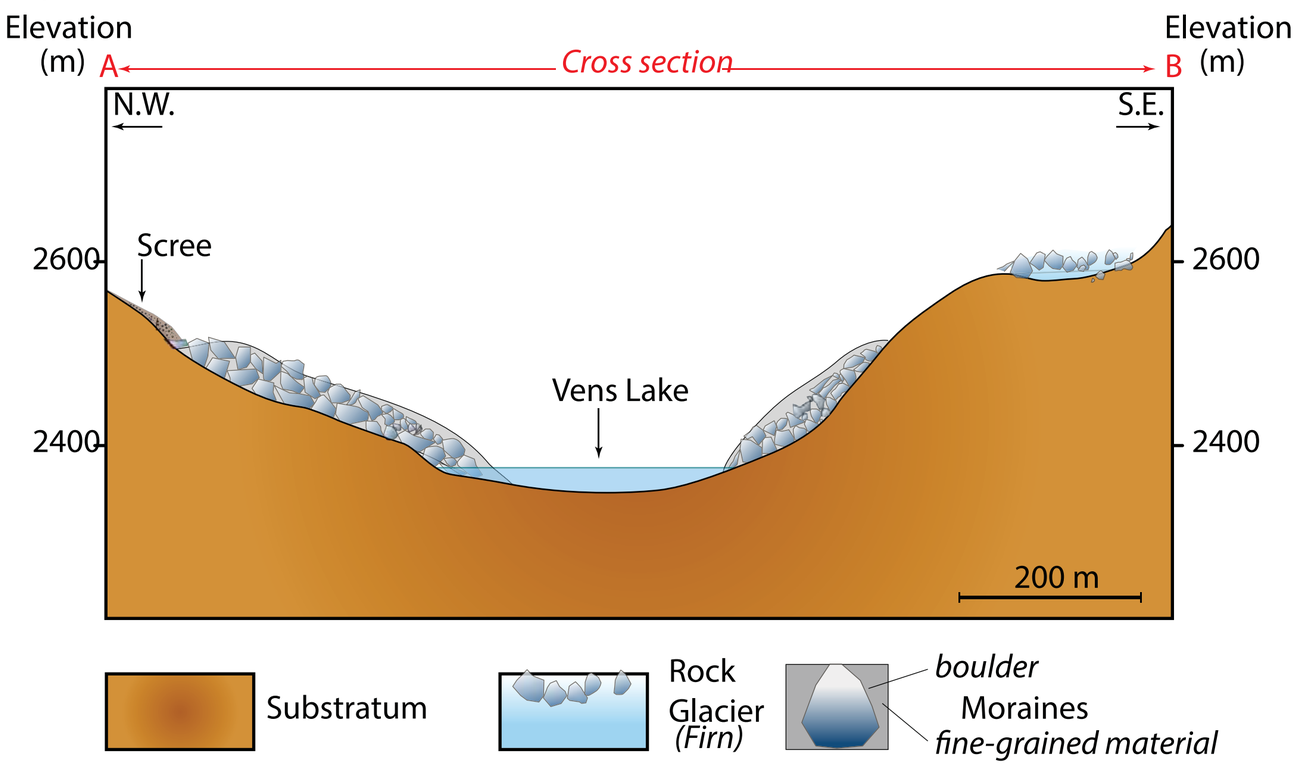

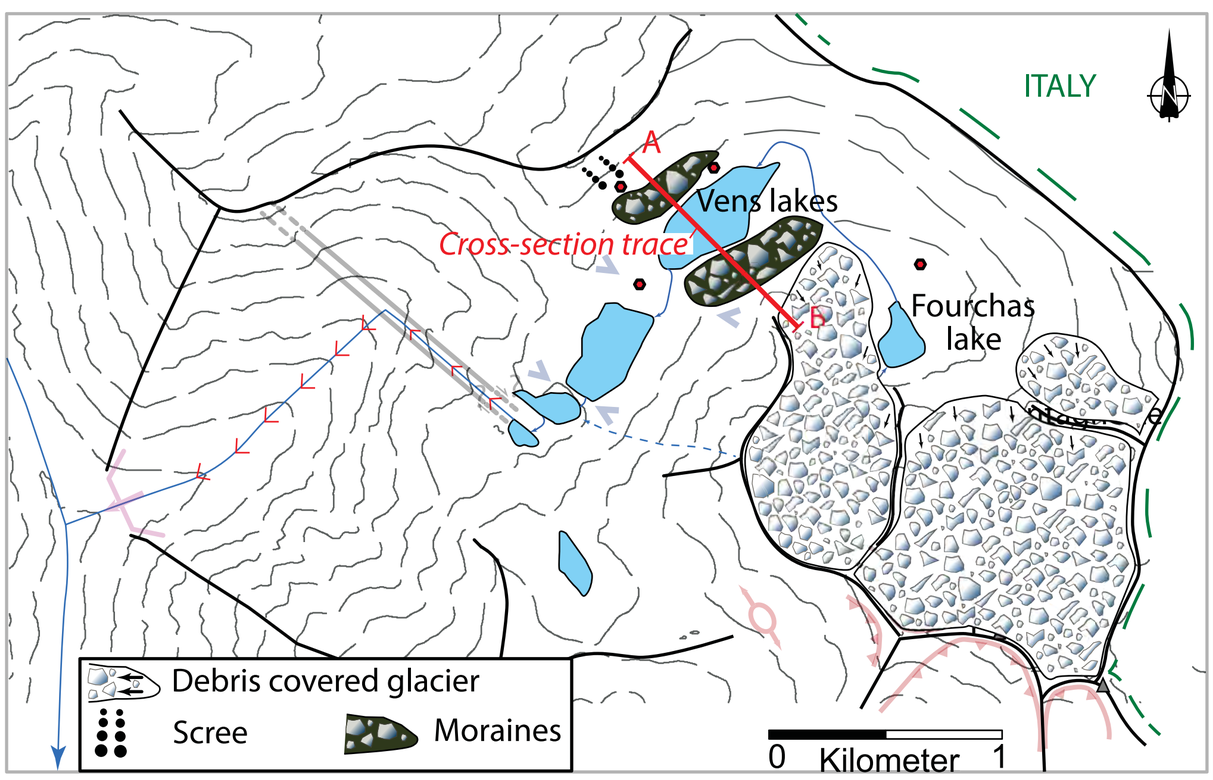

(D) 9-8 ka

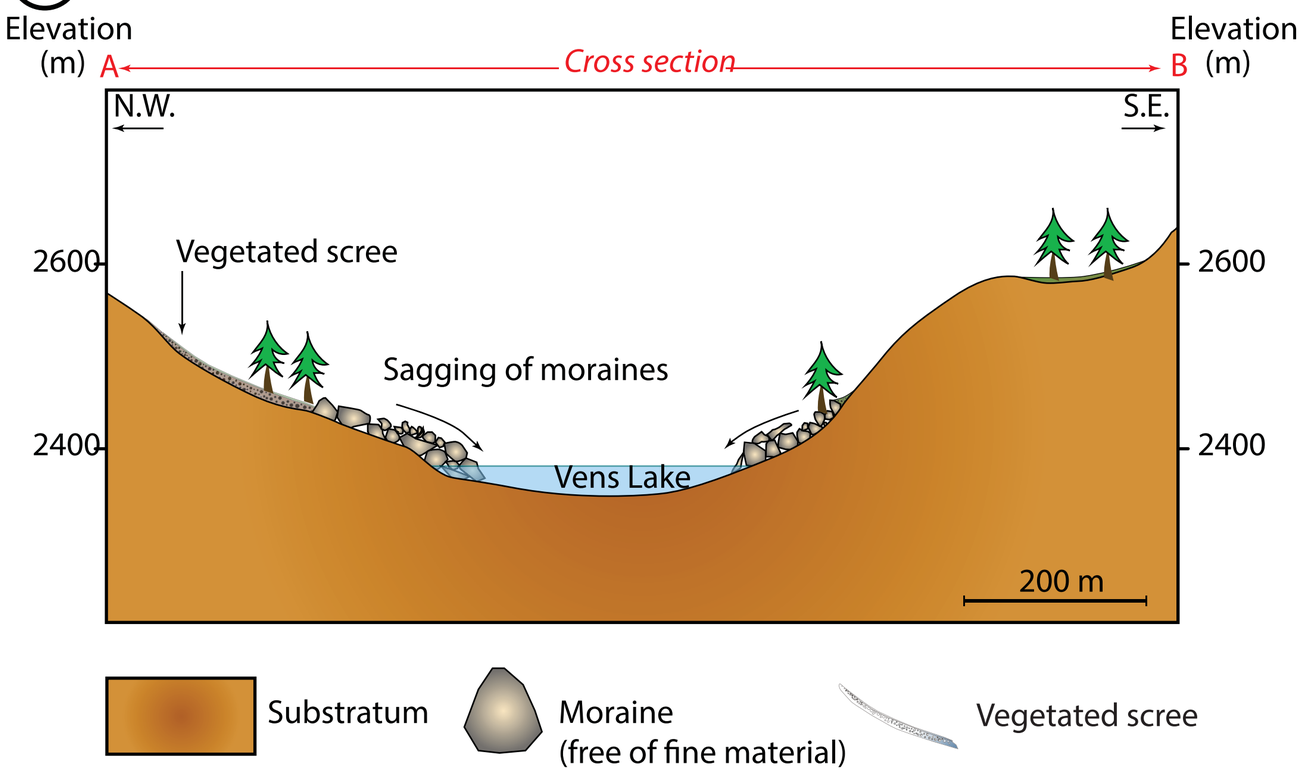

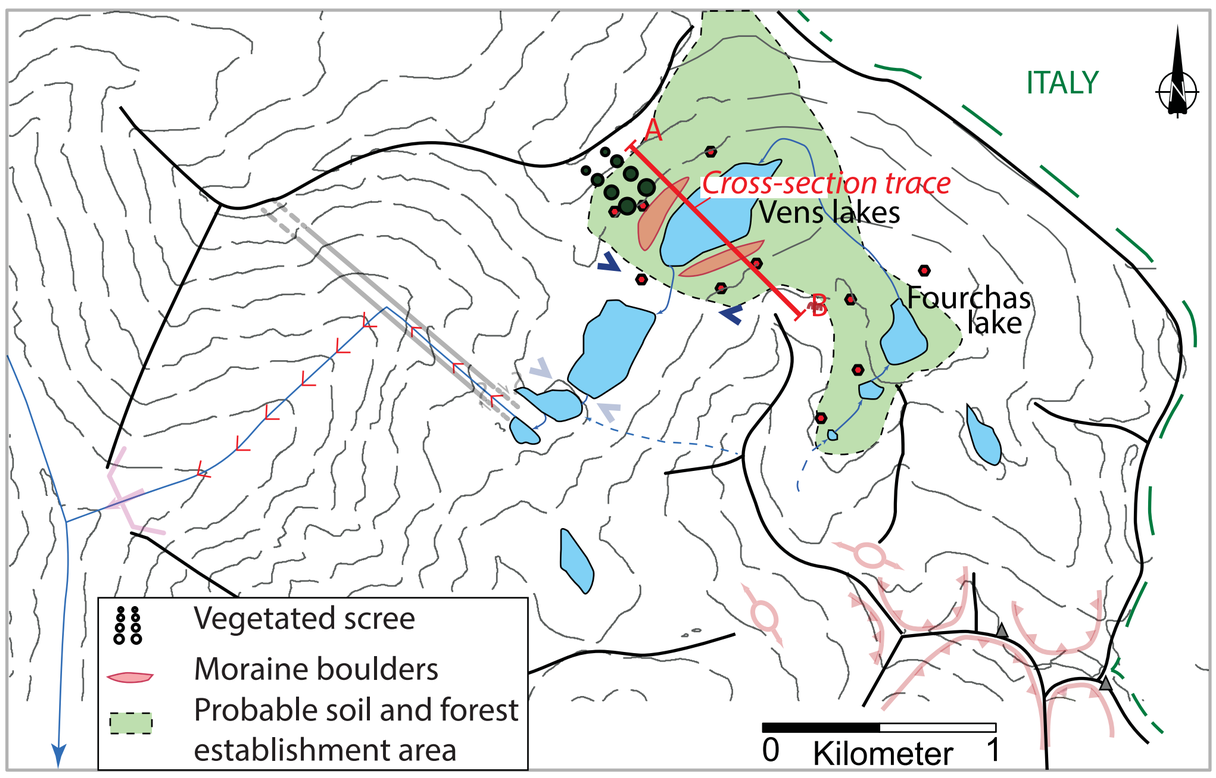

Table 1. ^{10}Be sample characteristics and exposure ages from the Vens Valley glacially polished surfaces.

Samples	Longitude	Latitude	Elevation	Dt[a]	Shielding factor[b]	Mass of quartz dissolved	[^{10}Be][c]	^{10}Be spike	^{10}Be/^{9}Be	^{10}Be	^{10}Be	^{10}Be age	σT_{min}/+5%	^{10}Be age
			(m)	*(cm)*		*(g)*	*(10^5 at/g)*	*(g)*	*(blank corrected)*	*(nb. atoms)*	*uncertainty (%)*	*(years)*		*(Snow corrected)*
Polished bedrock samples														
Fourchas Lake are (higher valley cirque)														
(Elevation: 2450 - 2600 m)														
Clap 57	N44.31315	E6.93588	2350	1.5	0.96	48.29	10.89	0.10132	2,58E-13	108851	3.3	6030 ± 205/365		7990 ± 359/639
Clap 62	N44.31128	E6.94464	2508	0	0.98	52.95	24.31	0.10104	6,30E-13	243124	3.0	9250 ± 290/546		12250 ± 384/723
Clap 63	N44.30612	E6.94256	2599	5	0.94	77.52	17.99	0.10112	6,87E-13	179940	3.7	7320 ± 278/459		9680 ± 368/608
Clap 66	N44.30862	E6.94525	2535	5	0.95	72.05	18.86	0.10837	6,69E-13	188639	3.9	7910 ± 317/507		10470 ± 420/671
Clap 67	N44.31102	E6.94428	2520	1	0.7	92.23	10.47	0.09944	4,44E-13	104674	8.3	6530 ± 545/635		8640 ± 721/840
Vens Lake area (Lower part of glaciated zone)														
(Elevation: 2350 - 2450 m)														
Clap 51	N44.31585	E6.93521	2352	1	0.95	34.16	13.21	0.09944	2,29E-13	132141	5	14680 ± 722/1030		-
Clap 52	N44.31621	E6.93458	2388	1	0.94	42.28	82.21	0.10106	1,74E-13	82206	8	4170 ± 341/400		4620 ± 378/443
Clap 54	N44.31709	E6.93662	2368	1	0.96	47.84	12.6	0.10089	2,99E-13	126008	4	6350 ± 234/394		7030 ± 259/437
Clap 56	N44.31338	E6.93608	2357	1.5	0.95	43.63	47.78	0.10163	1,05E-13	47784	100	2660 ± 2662/2665		2949 ± 2949/2952
Clap 58	N44.31382	E6.93330	2380	0.5	0.98	66.15	18.28	0.10144	5,93E-13	182818	3	8230 ± 256/485		9120 ± 284/537
Frontal Vens-I moraine boulder samples (Vens Lake area)														
Ve-18.01	N44.31484	E6.93389	2350	0	0.90	27,4546	9.326	0.1518	2.89E-13	256048	2.8	14240 ± 410/702		-
Ve-18.02	N44.31484	E6.93390	2355	1	0.90	19,4994	1.84	0.1495	4.20E-13	23081	2.0	14580 ± 330/586		-
Ve-18.03	N44.31483	E6.93392	2345	2	0.90	30,1421	12.079	0.1513	1.19E-13	364083	3.7	15320 ± 562/832		-

[a]Dt is the sample thickness.

[b] Azimuths and angular elevations (0-90°) to calculate the shielding factor were recorded using a compass and clinometer.

[c] All samples measured at the ASTER facility. AMS results are standardized to NIST_27900. ^{10}Be/^{9}Be ratios were corrected for a process blank value of 3.51 10^{-15}.

The presented production rates are scaled to the sampling coordinates following Stone (2000) from a sea-level high latitude ^{10}Be production rate of 4.02 atoms g^{-1} taking into account the revised ^{10}Be half-life (Chmeleff et al., 2010; Korschinek et al., 2010) and corrected for topographic shielding following Dunne et al. (1999), see Analytical Procedures section 4.2. Snow correction includes a 6-month cover of density 0.3 g.cm-3 (1.5 m of snow in Zone 1,and 0.5 m in Zone 2, except for Clap 52, sampled in a steep rock-wall). Errors are shown at 1 σ. They correspond to internal errors (left) and /an external errors with additional ~5% uncertainty linked to the production rate determination (right).

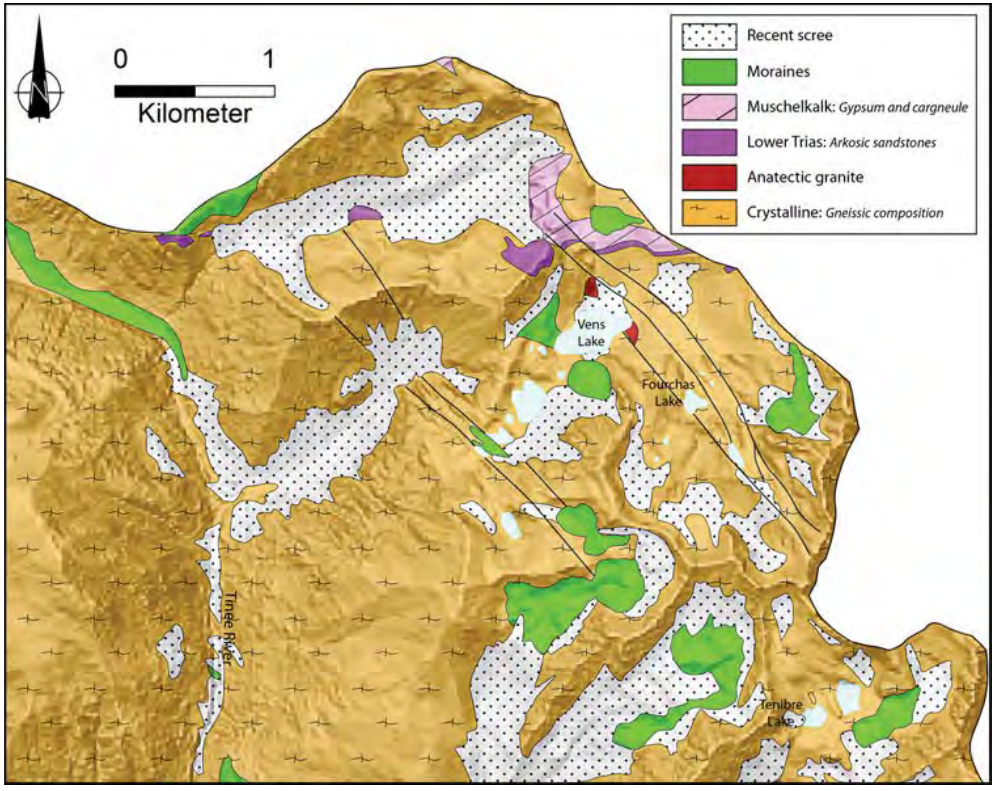
0
1
Kilometer
Recent scree
Moraines
Muschelkalk: Gypsum and cargneule
Lower Trias: Arkosic sandstones
Anatectic granite
Crystalline: Gneissic composition
Vens Lake
Fourchas Lake
Tenibre Lake
Tinee River

Suppl. Mat. Table 1. ^{10}Be sample characteristics and exposure ages from the Fer Valley glacially polished surfaces (recalculated ages from Darnnault et al., 2012).

Sample	Location	Lat (dec°)	Lon (dec°)	Alt (masl)	Conc (at/g)	1s (1E+04 at/g)	Shield. Corr	Density[1]	Thickness (cm)	Er. (cm/yr)	Scaling Factor	Age(ka)	1σ (ka)
Glacial polished surface													
Upper Slope (Elevation: 2700-2900 m)													
Clap 09	Lac Fer	N 44,27424	E 6,96350	2731	5,28E+05	2.0	0.86	2.75	5	0	7.94	19.71	0.44
Clap 10	Lac Fer	N 44,27448	E 6,96321	2701	4,93E+05	2.0	0.87	2.75	5	0	7.76	18.62	0.41
Clap 12	Lac Fer	N 44,27547	E 6,96536	2740	5,54E+05	1.8	0.94	2.75	5	0	7.96	18.88	0.42
Clap 14	Lac Fer	N 44,27510	E 6,96650	2814	6,24E+05	5.3	0.91	2.75	5	0	8.40	20.81	0.47
Lower Slope (Elevation: 2500-2700 m)													
Clap 03	Rabuons	N 44,26870	E 6,97861	2511	3,47E+05	1.0	0.87	2.75	5	0	6.76	15.02	0.33
Clap 07	Rabuons	N 44,26510	E 6,97671	2560	3,27E+05	1.0	0.85	2.75	5	0	6.94	14.09	0.32
Clap 18	Lac Fer	N 44,27375	E 6,96375	2642	1,90E+05	1.4	0.48	2.75	15	0	7.35	14.88	0.33
Clap 23	Lac Fer	N 44,27559	E 6,96455	2670	2,39E+05	1.5	0.55	2.75	5	0	7.48	14.81	0.33
Clap 24	Lac Fer	N 44,27468	E 6,96230	2620	2,80E+05	8.1	0.45	2.75	5	0	7.44	21.36	0.49
Clap 25	Lac Fer	N 44,27425	E 6,96171	2620	1,27E+05	1.2	0.45	2.75	5	0	7.09	10.11	0.23
Clap 26	Lac Fer	N 44,27407	E 6,96152	2604	5,59E+04	0.4	0.45	2.75	5	0	6.53	4.83	0.11
Fer 01	Lac Fer	N 44,27437	E 6,96090	2600	1,14E+05	1.2	0.72	2.75	5	0	6.68	6.01	0.13
Fer 02	Lac Fer	N 44,27440	E 6,96084	2590	1,34E+05	1.8	0.55	2.75	5	0	6.90	8.94	0.20
Fer 03	Lac Fer	N 44,27443	E 6,96089	2588	1,95E+05	1.8	0.72	2.75	5	0	6.93	9.91	0.22
Fer 05	Lac Fer	N 44,27442	E 6,96181	2645	2,72E+05	4.3	0.73	2.75	5	0	7.31	12.96	0.30
Fault zone													
Clap 15	Lac Fer	N 44,27454	E 6,96578	2786	7,68E+04	2.4	0.95	2.75	5	0	7.18	2.86	0.07
Clap 16	Lac Fer	N 44,27474	E 6,96468	2757	3,37E+05	1.0	0.96	2.75	5	0	7.81	11.43	0.26
Clap 17	Lac Fer	N 44,24439	E 6,96454	2770	2,93E+05	3.5	0.99	2.75	5	0	7.76	9.68	0.22
Clap 19	Lac Fer	N 44,27375	E 6,96375	2642	1,22E+05	1.5	0.48	2.75	15	0	7.17	9.78	0.22
Clap 20	Lac Fer	N 44,27375	E 6,96375	2642	2,08E+05	1.9	0.48	2.75	15	0	7.40	16.18	0.36
Clap 21	Lac Fer	N 44,27512	E 6,96349	2653	6,94E+04	0.8	0.62	2.75	5	0	6.66	4.27	0.10
Clap 22	Lac Fer	N 44,27546	E 6,96461	2663	1,70E+05	0.5	0.55	2.75	5	0	7.32	10.73	0.24

[1] Density of 2.75 is used accordingly to the Fer gneiss density